Exploring the impact of Cenomanian paleogeography and marine gateways on oceanic oxygen

Marie Laugié[1], Yannick Donnadieu[1], Jean-Baptiste Ladant[2], Laurent Bopp[3], Christian Ethé[4] and François Raisson[5].

[1]Aix Marseille Univ, CNRS, IRD, INRA, Coll. France, CEREGE, Aix-en-Provence, France
[2]Laboratoire des Sciences du Climat et de l'Environnement, LSCE/IPSL, CEA-CNRS-UVSQ, Université Paris-Saclay, 91191 Gif-sur-Yvette, France
[3]LMD/IPSL, Ecole Normale Supérieure / PSL University, CNRS, Ecole Polytechnique, Sorbonne Université- Paris, France
[4]Institut Pierre-Simon Laplace, Sorbonne Université/CNRS, Paris, France
[5]Total EP – New Exploration Concepts R&D Program, Pau, France

KEY POINTS

- Cenomanian paleogeography appears as a major long-term controller to install prerequisite conditions for Oceanic Anoxic Event 2 to occur.
- A deep connection between the Pacific and Central Atlantic oceans is needed before OAE2 to explain the Central Atlantic redox data.
- The reconstructed Cenomanian oceanic circulation is vigorous but does not prevent large parts of the ocean to be anoxic.

ABSTRACT

The Cenomanian-Turonian period recorded one of the largest disruptions to the oxygen and carbon cycles, the Oceanic Anoxic Event 2 (OAE2, 94 Ma). This event is global, yet paleo-reconstructions document heterogeneous ocean oxygenation states and sedimentary carbon contents, both temporally and spatially, suggesting that several mechanisms are at play. To better understand the long-term controls on oceanic oxygen and the initial oxygenation conditions prevailing at the beginning of OAE2, we perform numerical simulations of the Cenomanian using the IPSCL-CM5A2 Earth System Model, which includes a marine biogeochemistry component. We examine the control of the biogeochemical states of the global and Central Atlantic oceans by the depth of the Central American Seaway (CAS). The simulations show that a vigorous ocean circulation existed during the Cenomanian and that dysoxia/anoxia was caused by paleogeography rather than by ocean stagnation. The existence of restricted basins, disconnected from the deep global circulation and supplied with oxygen-depleted waters from Oxygen Minimum Zones of the surrounding basins, played a key role in the development of dysoxic/anoxic regions. A comparison with redox-proxy data suggests that a deep connection existed between the

Pacific and Central Atlantic prior to OAE2. A shallowing of the CAS may have contributed to the establishment of enhanced anoxia in the Central Atlantic during OAE2. The paleogeographic configuration and that of gateways and submarine topographic barriers appear as major long-term controllers of the oceanic circulation and oxygen distribution, leading to low-oxygen concentrations in extended parts of the ocean as prerequisite conditions for OAEs to occur.

1. Introduction

The Cenomanian-Turonian is a key period to study the oxygen and carbon cycles as it recorded one of their greatest disturbance, known as the Oceanic Anoxic Event 2 (OAE2) and characterized by the widespread deposition of organic-rich sediments (Arthur et al., 1987; Jenkyns, 2010; Owens et al., 2018). A positive carbon isotopic excursion (CIE) associated with OAE2 delimits the event in the lithological succession and shows that this event was global and rapid (<1 Myr; Sageman et al., 2006; Jenkyns, 2010; Gangl et al., 2019; Jones et al., 2019). However, the associated carbon enrichment is strongly variable, both spatially, with content of total organic carbon (TOC) varying between 0 to 50% during OAE2 (Owens et al., 2018), but also temporally, with sites documenting the onset of deposition of organic-rich sediments prior to OAE2, particularly in the Southern Central Atlantic (Kuypers et al., 2002; Montoya-Pino et al., 2010; Owens et al., 2012; Trabucho Alexandre et al., 2010; Westermann et al., 2014).

Proxy data of redox sensitive trace elements also document heterogeneous oxygenation state before and during OAE2 (Niels A. G. M. van Helmond et al., 2014), with some areas exhibiting for example anoxia before OAE2. A diachronism between CIE and carbon enrichment was also shown with highest TOC values prevailing before and after CIE, but not during (i.e indicating oxic conditions during OAE2), suggesting a partial decoupling of CIE and anoxia (Eldrett et al., 2014; Lowery et al., 2018). It has been suggested that the CIE was triggered by an abrupt and massive volcanism episode (Turgeon & Creaser, 2008; Du Vivier et al., 2014), driving an increase in atmospheric pCO_2 (Barclay et al., 2010; Bice et al., 2006) and an amplified hydrological cycle leading to increased nutrient inputs to the ocean (Blättler et al., 2011; N. A.G.M. Van Helmond et al., 2015; Niels A.G.M. van Helmond et al., 2014; Jenkyns et al., 2017; Nederbragt et al., 2004; Pogge Von Strandmann et al., 2013; Ruvalcaba Baroni et al., 2014). Other studies have shown that the CIE was also modulated by orbital controls determining the exact timing of its beginning and termination (Batenburg et

al., 2016; Li et al., 2017; Mitchell et al., 2008; Wagner et al., 2004). The decoupling of CIE and anoxia, as well as the spatial and temporal variations in carbon content and ocean redox conditions suggest that other mechanisms, in the longer term, are at play and act on temporal and spatial scales different from those suggested for CIE alone.

Unravelling the short-term controls on oxygenation and carbon burial during the OAEs appears thus challenging without a good understanding of the long-term control on oceanic oxygen and of the oxygenation conditions that existed at the beginning of the OAEs. The Cretaceous ocean has long been considered stratified and stagnant, due to the coeval greenhouse climate (Degens & Stoffers, 1976; Erbacher et al., 2001; Sinninghe Damste & Koster, 1998). Such a sluggish circulation was invoked to explain sea-floor anoxia and black shale deposition, but more recent observational and modelling studies have shown that a vigorous oceanic circulation was in place, with an active ventilation of the deep-ocean (Yannick Donnadieu et al., 2016; Ladant et al., 2020; MacLeod et al., 2008; Martin et al., 2012; Monteiro et al., 2012; Mourlot et al., 2018; Chris J Poulsen et al., 1998; Soares et al., 2014; Thiéblemont et al., 2020; Trabucho Alexandre et al., 2010; Du Vivier et al., 2014; Zheng et al., 2013). Other controls, such as long-term changes in paleogeography and in particular in the geometry of marine gateways, have thus been invoked to explain changes in oceanic circulation and ocean deoxygenation (Yannick Donnadieu et al., 2016; W. Dummann et al., 2020; Christopher J. Poulsen et al., 2001; Trabucho Alexandre et al., 2010). Dummann et al. (2020b) have in particular demonstrated that the shallow Falkland Plateau and Maurice Ewing Bank exerted a first-order control on ocean anoxia during the OAE1 in the Southern Atlantic, by providing favorable conditions without which organic carbon burial would not be possible during OAE1 (Wolf Dummann et al., 2020).

During the Cenomanian-Turonian, the Central Atlantic basin, from where numerous data document OAE2, is surrounded by five gateways, namely the Equatorial Atlantic Gateway (EAG) in the South, the CAS in the West, the Western Interior Seaway (WIS) in the North-West, the East Greenland Seaway (EGS) in the North-East and the Tethys Seaway in the East (Fig. 1). The paleodepths of the WIS, EGS and EAG are relatively well-constrained, with very shallow bathymetry for the WIS and EGS (<200 meters; Martinson et al., 1998; Gernigon et al., 2020) and shallow bathymetry for the EAG (<800 meters; Ye et al., 2017). The Tethys Seaway paleodepth is more uncertain (Nouri et al., 2016), as well as the paleodepth of the CAS that is suggested to vary concomitantly to OAE2 due to the Caribbean Large Igneous Province (CLIP) activity and the formation of the Caribbean Plateau (Buchs et al., 2018). There is some evidence supporting a causal relationship between the intense

volcanic activity associated with the CLIP development in the Late Cenomanian and the OAE2 (Joo et al., 2020; Turgeon & Creaser, 2008). Recent work also demonstrated that the depth of the CAS can exert a significant role on the oceanic circulation during the Cretaceous (Y. Donnadieu et al., 2006; Yannick Donnadieu et al., 2016; Ladant et al., 2020; Monteiro et al., 2012; Topper et al., 2011; Trabucho Alexandre et al., 2010) and, consequently, can strongly impact the distribution of dissolved oxygen in the ocean (Kerr & Kerr, 1998) and affect rates of organic matter preservation (Monteiro et al., 2012). Although it is unlikely that changes in gateway bathymetry are directly responsible for triggering OAE2 because they act on longer timescales, changes in the CAS depth and geometry on the runup to OAE2 may have preconditioned and/or contributed to the establishment of anoxic conditions in the deep Central Atlantic Ocean through a reorganization of deep-ocean currents. To date, however, the dynamics of oceanic oxygen during the Cenomanian and OAE2 has only been investigated using box models (Flögel et al., 2011; Ruvalcaba Baroni et al., 2014) and Earth System Models of Intermediate Complexity (EMIC; Monteiro et al., 2012).

Here, we examine the sensitivity of oceanic dissolved oxygen to a mid-Cretaceous paleogeography and to the CAS geometry using numerical simulations of the Cenomanian ocean with the IPSL-CM5A2 Earth System Model (ESM) (Sepulchre et al., 2020), which includes the marine biogeochemistry model PISCES (Aumont et al., 2015). We first analyze the long-term impact of a baseline Cenomanian-Turonian paleogeography (with the CAS open to deep circulation) on oceanic circulation and oxygen at the global scale. In a second step, we test the impact of changes in ocean dynamics on dissolved oxygen by performing two sensitivity experiments with intermediate and shallow CAS configurations. Results are focused on the Central Atlantic to investigate the consequences on dissolved oxygen of oceanic circulation changes arising from the different gateway geometries. Finally, the comparison with redox proxy data provides a better understanding of the long-term paleogeographic control on oceanic oxygen during the Cenomanian, as well as an estimate of the pre-OAE2 oxygenation state, which will serve as a basis for further unraveling the triggering mechanisms of OAE2 and the associated strong carbon burial.

2. Model description and experimental design

2.1 IPSL-CM5A2 Earth System Model

The IPSL-CM5A2 Earth System Model (Sepulchre et al., 2020) is an updated version of IPSL-CM5A-LR developed at IPSL (Institut Pierre-Simon Laplace) within the CMIP5 framework (Dufresne et al., 2013). IPSL-CM5A2 is composed of the LMDZ atmospheric model (Hourdin et al., 2013), the ORCHIDEE land surface and vegetation model (including the continental hydrological cycle, vegetation and the land carbon cycle; Krinner et al., 2005), and the NEMO ocean model (Madec and the NEMO Team, 2008), including the LIM2 sea-ice model (Fichefet & Maqueda, 1997) and the PISCES-v2 marine biogeochemistry model (Aumont et al., 2015). The ocean and atmospheric components are synchronized via the OASIS coupler (Valcke et al., 2006) and the XIOS input/output parallel library is used to read and write data. The atmospheric grid has a horizontal resolution of 96x95, (equivalent to 3.75° in longitude and 1.875° in latitude) and 39 uneven vertical levels. ORCHIDEE shares the same horizontal resolution, whereas the oceanic grid has 31 uneven vertical levels (from 10m width at the surface to 500m at the bottom) and a nominal horizontal resolution of 2°, enhanced to up to 0.5° in latitude in the 20°S-20°N latitudinal band. NEMO uses a tripolar grid to overcome the North Pole singularity (Madec & Imbard, 1996). For a more detailed description of the model and its different components, see Sepulchre et al. (2020).

2.2 PISCES marine biogeochemistry model

The PISCES model (Pelagic Interactions Scheme for Carbon and Ecosystem Studies, Aumont et al., 2015) simulates the lower trophic levels of marine ecosystems (nanophytoplankton, diatoms, microzooplankton and mesozooplankton), carbonate chemistry and the biogeochemical cycles of carbon, oxygen, and of the main nutrients: phosphorus, nitrogen, iron and silica. In PISCES, dissolved oxygen is produced in the ocean according to phytoplankton net primary production and consumed by zooplankton heterotrophic respiration, oxic remineralization of organic matter and nitrification (see Aumont et al. [2015] for detailed equations of all these terms). Dissolved oxygen is also exchanged at the air-sea interface using the parameterization of Wanninkhof (1992). Note that the atmospheric concentration of di-oxygen is set to a fixed ratio of 0.21. As in Bopp et al. (2017), we decompose dissolved oxygen into the O_2 saturation (O_2sat) and Apparent Oxygen Utilization (AOU) components. O_2sat only depends on seawater temperature and salinity. At the surface of the ocean, the concentration of dissolved oxygen is very close to its saturation state, such that $[O_2] = O_2$sat. AOU represents the quantity of oxygen that has been consumed by biogeochemical processes on the trajectory of a given water-mass from the ocean's surface,

and thus integrates both a biological and a ventilation signature. The three terms are linked as follows : $[O_2] = O_2sat – AOU$ (Bopp et al., 2017). We also used an additional inert artificial tracer allowing to compute the age of water masses, corresponding to the time spent since last surface contact (Bopp et al., 2017).

2.3 Experimental design

2.3.1 Boundary and Initial conditions

The baseline and sensitivity simulations share the Cenomanian-Turonian (CT) land–sea configuration (Fig.1) of Sewall et al. (2007), in which the bathymetry from Müller et al. (2008) is implemented, in order to represent deep-oceanic topographic features, such as ridges, that are absent from the Sewall paleogeographic configuration. The pCO_2 concentration is fixed at 1120 ppm, i.e. 4 times the pre-industrial atmospheric level (PAL), which is a value suggested by CT pCO_2 reconstructions (e.g., Wang et al., 2014), and which has been shown to reasonably reproduce the mean CT climate in IPSL-CM5A2 simulations (Laugié et al., 2020). Vegetation is assigned along latitudinal bands as described in Laugié et al. (2020) and a mean soil color and texture is prescribed uniformly to all continents. Polar ice sheets are removed and replaced by a brown bare soil after adjusting the topography to account for isostatic rebound. The solar constant is reduced to a CT value of 1353.36 $W.m^{-2}$ (Gough, 1981). Orbital parameters are kept at their modern value. The global budgets of all macro-nutrients (nitrate, phosphate and silicate) in the oceans are also kept identical to the modern ones. We deliberately choose to keep these budgets constant in order to isolate the effect of ocean dynamics on the intensity of ocean anoxia while mimicking the tectonic drift of the CLIP across the Central American seaways by shallowing the depth of the gateway.

The three simulations present different paleobathymetric configurations for the Central American Seaway (CAS; Fig. 1). The baseline *DeepCAS* simulation exhibits a deep connection (~ 4000 m depth) between the Pacific and Central Atlantic (Fig. 1). The CAS depth is reduced to intermediate (~ 2500 m) and shallow depths (~ 300 m) in the *IntermediateCAS* and *ShallowCAS* simulations, respectively (Fig. 1). All other boundary conditions are identical for the three simulations. The simulations are initialized with warm idealized conditions adapted from those described in Lunt et al. (2017). The constant initial salinity field is set to 34.7 PSU, and ocean temperatures are initialized with the depth-dependent distribution of

Laugié et al. (2020).

2.3.2 Equilibrium state

The baseline DeepCAS simulation is first run for 3000 years with IPSL-CM5A2. From the end state of this first simulation, we branch the two CAS sensitivity simulations and integrate them for 3500 years. The baseline simulation is also extended for another 3500 years. Finally, because the biogeochemical equilibrium of the ocean typically requires a longer spin-up (Séférian et al., 2016), we extend each simulation over an additional 3000-year period by performing "offline" PISCES-only simulations. In those offline simulations, PISCES is forced by using the last 100-year climatology (e.g., monthly means of ocean temperature, salinity, currents, incoming radiation, ….) from each of the 3 coupled climate simulations. This strategy allows deep-ocean biogeochemistry, and in particular seafloor oxygen concentrations, to reach a final state closer to equilibrium. Climate and biogeochemical results are discussed using climatological averages calculated over the last 100 years of IPSL-CM5A2 and PISCES integrations, respectively.

The equilibrium for the three IPSL-CM5A2 simulations is assessed using surface and deep oceanic temperatures (Supplementary Fig.S1a,b) and the intensity of the global meridional stream function (Supplementary Fig.S1c). Both surface and deep temperatures have reached a near equilibrium state with temporal drifts estimated at less than 0.05°C/century (Supplementary Table 1) during the last 1000 years of the climate model integration. The meridional streamfunction is also well equilibrated with stable maximum intensity of around 17 Sv during the last 2000 years of the simulation.

Furthermore, the three PISCES simulations exhibit negligible drifts in deep ocean oxygen concentrations (Supplementary Fig.1d) after 3000 years of offline simulations (Supplementary Table 1; <0.1 mmol/m^3/century).

2.4 Redox data

The simulated results are compared to reconstructions of oceanic oxygen state inferred from pre-OAE2 and OAE2 data. Our data compilation is built from the databases of Monteiro et al. (2012) and Owens et al. (2018). The oxygenation states documented in these two databases are essentially inferred from TOC values, which are a function of bottom water oxygen, but are also influenced by other parameters such as the organic matter flux to the seafloor, the dilution with inorganic matter or diagenetic processes. In our compilation, we thus selected only data points for which other indicators than TOC were available, such as

analysis of redox sensitive trace elements or presence/absence of benthic biota, which are direct indicators of bottom water oxygenation. We also chose to only select data for which an estimation of the paleowater depth exists in order to be comparable with our model results. The data points are distributed to their paleolocation using the GPlates software (Qin et al., 2012) and the global plate rotation model of Scotese (2016). In case of an inconsistency between the calculated paleoposition and the paleowater depth, data points are then moved to the nearest location with a correct paleodepth in the model (See Supplementary information).

3. Results

In a first step, we describe the major patterns of ocean circulation and oxygen distribution at the global scale, using the *DeepCAS* simulation. Results from the *IntermediateCAS* and *ShallowCAS* simulations are very similar to DeepCAS at the global scale, with the change in CAS depth mostly affecting the Central Atlantic. In a second step, we focus on the Central Atlantic and analyze the regional impact of the CAS on ocean circulation and oxygen distribution in the three simulations.

3.1 Ocean circulation and oxygen distribution in the global ocean

3.1.1 Upper and intermediate ocean

Upper ocean waters (0-100 meters) are generally close to dissolved oxygen saturation, which means that oxygen concentrations are mainly determined by surface temperature and its influence on oxygen solubility (Fig. 2a). The Cenomanian upper ocean is characterized by elevated temperatures and a reduced equator-to-pole gradient (Laugié et al., 2020; Norris et al., 2002; O'Brien et al., 2017; Robinson et al., 2019; Tabor et al., 2016). In the tropical area, O_2 saturation is reduced to an average of 198 mmol/m^3 because oxygen solubility decreases with temperature. In comparison, the mean temperature in the tropical ocean in the pre-industrial simulation of Laugié et al. (2020) is 22.2°C, with a corresponding O_2 saturation at 228 mmol/m^3. In the high latitudes, O2 saturation reaches higher values (~300 mmol/m^3) than in the low latitudes but, again, with a large offset compared to preindustrial high-latitude saturation levels (~370 mmol/m^3). Subsurface oxygen concentrations (< 600 meters of water depth) also exhibit a latitudinal gradient (Fig. 2b) but they are more impacted by ocean dynamics, in particular in regions of strong vertical currents (e.g., equatorial upwelling, Fig. 2b). Specifically, in the Central Atlantic and Eastern Equatorial Pacific, the model simulates complete anoxia in the subsurface and up to the base of the photic zone. At

intermediate depths (600-1600 meters of water depth), oxygen concentration is globally more homogeneous in the ocean except in the South Pacific and Central Atlantic (Fig. 2c). South Pacific waters remain well-oxygenated from the surface to the bottom because this region is the source of deep-water in our Cenomanian simulations. In contrast, the Central Atlantic is bathed by oxygen-depleted waters (Fig. 2c), whose origin is described in more details in Section 3.2.

3.1.2 Deep Ocean

The deep-sea oxygen distribution is controlled at first order by the location of deep-water formation sites and by the bathymetry (Fig. 3a). In our simulations, deep-water formation sites are only located in the South Pacific Ocean, although intermediate-water formation takes place in the North Pacific Ocean (Fig. 2c). The South Pacific deep convection feeds a global meridional overturning circulation (MOC) of maximum intensity at ~18 Sv, similar to the modern Atlantic MOC (18 Sv; Talley et al., 2003). Note that the intensity of the MOC appears only weakly sensitive to the depth of the CAS (Supplementary Fig.S2). The simulated Cenomanian MOC reaches the abyssal ocean and suggests that the Cenomanian global circulation was vigorous, contrary to the well-anchored image of a sluggish ocean but in agreement with results from other recent model simulations (Yannick Donnadieu et al., 2016; Ladant et al., 2020; Trabucho Alexandre et al., 2010).

From their origin in deep-water formation sites in the South Pacific, deep waters flow northward into the Neotethys and Equatorial Pacific Oceans (Fig.3a). The deep Neotethys waters then circulate back to the Pacific to flow north of the mid-Pacific ridge and toward the North-Eastern Pacific. Pacific deep waters ultimately end up in the Central Atlantic whereas the deep South Atlantic is restricted from the global circulation by four submarine topographic barriers that are the Kerguelen Plateau, the Davie Ridge, the Equatorial Atlantic Gateway and the Drake passage (Fig. 3a). This pattern of deep circulation leads to interbasin gradients in deep ocean oxygen concentrations and water mass age (Fig. 3b); the degree of oxygenation of deep waters appearing well correlated with their age (Fig.4; Supplementary Fig.S3). The younger and most oxygenated waters are indeed found in the South Pacific and in the Neotethys Ocean. The South Atlantic and North-Eastern Pacific exhibit reduced oxygenation and older water masses, and the Central Atlantic is the oldest and most oxygen-depleted deep basin. The disconnection of the South Atlantic from the global deep circulation also explains the presence of old and oxygen-depleted water masses in this basin (Fig. 3b).

Interestingly, a similarly restricted deep circulation, confined to the Pacific and Neotethys Oceans due to bathymetric barriers, is also simulated in a Cenomanian simulation with the CCSM4 ESM (Ladant et al., 2020), suggesting that submarine topographic barriers are major controllers of the deep circulation and thus of dissolved oxygen in the deep ocean.

3.1.3 Relationship between oxygen and marine productivity

In our simulations, there is an obvious correlation between ocean dynamics and deep ocean oxygenation (Fig. 4), indicating that older waters are the most oxygen-depleted ones. There is not such a clear correlation between marine productivity and deep oxygen concentrations, but interesting insights can be drawn from oxygen-productivity cross plots calculated in different regions of the ocean (shown on Fig. 4b) with distinct oxygen dynamics in the water column (Fig. 5).

The meridional surface oxygen gradient is evident from the vertical oxygen profiles (Fig. 5a). High latitudes locations (Profiles 1 and 3) exhibit high oxygen levels in the surface due to low temperatures whereas lower-latitude profiles show lower surface values (Profiles 2,4,5,6).

Profile 1 is located in a deep-water formation area, with a low marine productivity. Deep-convection brings oxygen down to seafloor, and high oxygen values are found throughout the whole water column (Fig. 5a). In contrast, albeit at the same latitude but in the Northern Hemisphere, the Profile 3 is located close to a region of intermediate water formation with seasonal primary production (Fig. 5b,c). Limited convection and slightly higher productivity values impose a strong vertical gradient in oxygen between 300 and 1000 m and reduces intermediate to deep oxygen levels. Nonetheless, these two regions can be viewed as “low productivity – high oxygen” areas.

Profile 2 and 6 are located in the subtropics in low productivity areas (Fig.5c). Marine productivity is low because of poor nutrient availability, which limits carbon export and oxygen consumption at depth. However, elevated upper ocean temperatures reducing O_2 saturation leads to moderate surface and intermediate oxygen levels (“low productivity – low oxygen” region). In the deep ocean, those 2 oxygen profiles display a divergent trend. Profile 2 is located directly north of the deep-water formation area, from where oxygenated waters circulate. Oxygen concentrations in Profile 2, therefore, increase below ~ 2300 m (Fig. 5a). Profile 6 is instead located in the South Atlantic away from well-oxygenated deep-water

sources, which explains the continuous decrease of oxygen concentrations with depth (Fig. 5a).

In contrast to the profiles discussed above, which are located in open ocean sectors of the Pacific and South Atlantic Oceans, Profiles 4 and 5 are more representative of coastal settings of the Central Atlantic basin. At these two locations, marine productivity is very high and leads to an intense export of organic matter and high oxygen utilization at depth. Hence, intermediate and deep ocean oxygen concentrations fall below the hypoxic threshold and, for Profile 5, even below the anoxia threshold ("high productivity – low oxygen" regions). The differences between both profiles are explained by vertical ocean dynamics (Supplementary Fig. S4). Profile 5 is indeed located in a major upwelling area whereas the site of Profile 4 experiences seasonal deepening of the mixed-layer and is thus a sinking area for upper ocean waters. Waters remain oxic only above 100 m in Profile 5 because upwelling supplies nutrient-rich and oxygen-depleted waters to the surface (Supplementary Fig.S5), which fuels productivity and enhances oxygen depletion. At the location of Profile 4, deep coastal upwellings also allow nutrient-rich waters to reach the photic zone but the seasonal MLD deepening carries dissolved oxygen down the water column, which increases the remineralization potential. Increased remineralization increases the nutrient supply and boosts marine primary production to levels higher than at Profile 5. Deeper in the water column, both sites are bathed by intermediate and deep waters originating from the Pacific and exhibit similar oxygen concentrations. However, these last findings about Profiles 4 and 5, and the oxygen dynamics in the Central Atlantic more generally, are meaningful in a context of CAS open to deep circulation but are significantly altered with a shallower CAS configuration, as we now examine.

3.2 Central Atlantic circulation

We now focus on the Central Atlantic circulation and distinguish three depth intervals: upper ocean circulation (<600 meters of water depth), intermediate circulation (600 – 1600 meters of water depth) and deep circulation (> 1600 of water depth). Inflow and ouflow water fluxes are computed along the five gateways surrounding the Central Atlantic Ocean: the CAS, the EAG, the WIS, the EGS and the Tethys Seaway (Fig.1).

3.2.1 Upper ocean circulation (0-600 meters)

Fig.6 depicts the upper ocean circulation of the Central Atlantic, showing the directions of major currents in and out of the Central Atlantic (Fig.6a) and the corresponding

water fluxes (Fig.6b). Most of the horizontal circulation is dominated by a westward current, the circum-equatorial current, flowing through the Central Atlantic from the Tethys Seaway (main inflow) to the CAS (main outflow). Similar patterns of upper ocean circulation were simulated in previous modeling studies (Yannick Donnadieu et al., 2016; Topper et al., 2011; Trabucho Alexandre et al., 2010). Minor counter-currents also flow into the Central Atlantic across the CAS and the EAG. The circum-equatorial upper ocean current separates the basin into two distinct areas: an upwelling area in the southern Central Atlantic, strongly influenced by underlying older waters, and a downwelling area in the northern Central Atlantic, in which the thermocline deepens with mixed layer depth reaching 350 m. High marine productivity is simulated in these areas of strong water mixing regardless of the CAS configuration (See Supplementary Fig.S6). In contrast, though the upper ocean circulation is very similar, the intensity of water fluxes through the CAS is smaller for the *ShallowCAS* simulation, due to the reduced water depth (Fig.6b). Incoming and outgoing fluxes are approximatively halved in the *ShallowCAS* simulation compared to the *IntermediateCAS* and *DeepCAS* simulations.

3.2.2 Intermediate circulation (600-1600 meters)

The intermediate currents system in the Central Atlantic is similar in the *DeepCAS* and *IntermediateCAS* simulations (Fig. 7a and 7c). The largest incoming water flux comes from the Pacific through the CAS in the deeper intermediate layers. This estuarine circulation between the Pacific and the Central Atlantic is comparable to that suggested by previous model studies (Yannick Donnadieu et al., 2016; Monteiro et al., 2012; Topper et al., 2011; Trabucho Alexandre et al., 2010) and explains the latitudinal gradient in water mass properties in the Central Atlantic (Supplementary Fig.S7). The southern part of the basin is under the influence of both intermediate waters coming from the eastern Equatorial Pacific and upwelled waters from the deep Central Atlantic (Fig.7 and Supplementary Fig.S7). As a result, the intermediate southern Central Atlantic is bathed by colder, fresher and older waters than in the northern Central Atlantic, whose intermediate water mass composition includes a greater proportion of warmer, saltier and younger waters originating from the Neotethys and from sinking waters (Supplementary Fig.S7).

On the contrary, the *ShallowCAS* simulation exhibits a different intermediate circulation (Figs. 7b and 7d) because the depth of the CAS prevents intermediate currents to flow across it. The inflow water transport from the Neotethys more than doubles compared to the DeepCAS and IntermediateCAS, and intermediate waters originating from the EAG start flowing into the Central Atlantic. Without the influence of Pacific intermediate and deep

waters, Central Atlantic intermediate waters are then globally younger and warmer in the *ShallowCAS* simulation than they are in the two other simulations (Supplementary Fig.S7).

3.2.3 Deep circulation (> 1600 meters)

The deep circulation is different for the three CAS configurations (Fig. 8). The *DeepCAS* and *IntermediateCAS* simulations exhibit water exchange only through the CAS because the depth of the other gateways is less than 1600 meters. The deep Central Atlantic is thus bathed by deep and cold waters from the Pacific. The *IntermediateCAS* configuration (2500 m depth maximum) limits inflows and outflows to half that of the DeepCAS simulation, and prevents the deepest waters (below 2500 meters) of the Pacific from entering the Central Atlantic. In contrast, in the ShallowCAS configuration, each gateway enclosing the Central Atlantic is closed to deep circulation. The deep Central Atlantic is instead supplied with waters from intermediate levels. In particular, warm intermediate waters coming from the EAG represent a significant contribution to deep Central Atlantic waters, as indicated by the water age (Fig. 9). As a consequence, the deep Central Atlantic presents much warmer waters compared to the two previous simulations (13.6°C vs 8.7°C and 9°C for *DeepCAS* and *IntermediateCAS* simulations, respectively).

3.3 Central Atlantic oxygenation

The changes in ocean circulation with CAS configuration in the Central Atlantic leads to different oxygenation states at the seafloor (Fig. 10). Regions of intermediate and deep depths present a decreasing oxygen content with the shallowing of the CAS. They evolve from a hypoxic or oxic state in the *DeepCAS* simulation, to an anoxic or hypoxic state in the *IntermediateCAS* simulation and to complete anoxia in the *ShallowCAS* simulation (oxic = $[O_2] > 62.5$ mmol/m^3; hypoxic = $6.5 < [O_2] < 62.5$ mmol/m^3; anoxic = $[O_2] < 6.5$ mmol/m^3). This oxygen-depletion trend is directly linked to the origin of waters bathing the intermediate and deep parts of the basin (Fig. 10 and Supplementary Fig.S8). With a deep CAS, the Central Atlantic is supplied with well-oxygenated deep waters from the Pacific. With an intermediate CAS, the Central Atlantic is supplied with more hypoxic intermediate waters from the Pacific. Finally, with a shallow CAS, the Central Atlantic is mostly supplied with anoxic shallow waters from the Equatorial Atlantic Gateway. The CAS, therefore, acts as a submarine topographic barrier for both currents and oxygen and, if shallow enough, can be responsible for complete marine anoxia at a basin-scale despite the existence of an active circulation.

4. Discussion

Our compilation of redox data (See supplementary data) indicates the ocean oxygenation state before (Fig. 11a) and during OAE2 (Fig. 11b), allowing identifying heterogeneous conditions both spatially and temporally. Before OAE2, most of the ocean was oxic, except some areas located in the Central Atlantic (Fig.11a, Southern Central Atlantic, Southern WIS, deepest part of Gulf of Mexico). During OAE2 (Fig.11b), redox data indicates an expansion of the anoxia to the whole Central Atlantic, with some locations showing fluctuations from oxic to hypoxic/anoxic conditions (e.g. in the WIS, Northern Central Atlantic, Moroccan margin). Outside the Central Atlantic, the hypoxia/anoxia extends to the Southern Atlantic and to the Neotethys (deep outer shelves or even some parts of the deep basin), with fluctuations between oxic and anoxic conditions also reconstructed in some locations. In the easternmost part of the South Neotethys (e.g North Indian, Kerguelen plateau) as well as in the Northern Pacific coasts, hypoxia is sometimes reached during OAE2, but in alternation with oxic conditions. Finally, the Southern Pacific always stays oxic.

In the following, we compare our modelling results to these oxygenation trends for the pre-OAE and OAE2 periods, in a first step at the global scale, and in a second step with a focus on the Central Atlantic, in order to investigate the question of the CAS paleobathymetry.

1.1 The pre-OAE2 oxygenation state: a data/model comparison

Outside the Central Atlantic, the results predicted by our three Cenomanian simulations agree well with reconstructions of oceanic oxygen state inferred from data for pre-OAE2, as illustrated in the DeepCAS simulation (Fig. 11a). Most of the sites suggest sedimentary burial in oxic conditions and the model consistently reproduces a well-oxygenated seafloor at the site locations. Simulated dissolved oxygen concentrations show that these oxic environments exhibit a large range of values, from 62.5 mmol/m^3 (dysoxia limit) to more than 300 mmol/m^3 but, unfortunately, proxies only discriminate anoxic/dysoxic from oxic conditions and rarely allow to reconstruct the absolute oxygen concentration in oxic environments. However, it is interesting that all sites that shift from an oxic to a hypoxic or anoxic environment during OAE2 (Fig 11.b) are located in areas where the model simulates moderate oxygenation for the pre-OAE2 (e.g., Southern Atlantic, Tethyan continental slopes, North-Eastern Africa, [O_2] ~< 120 mmol/m^3) driven by basin restriction and/or reduced O_2

484 saturation due to elevated temperatures. Other sites that remain oxic or dysoxic during OAE2
485 are found in more-oxygenated areas during pre-OAE2 (North-Eastern/North-Western-Central
486 Pacific, shallow Tethyan and Tibetan platforms, Kerguelen plateau, $[O_2]$ > 150 mmol/m^3).
487 Finally, the New Zealand site is interesting in that neither the model nor proxy records
488 document any major change in oxygen concentrations during OAE2, which agrees with the
489 site location in an area of deep-water formation ensuring high simulated oxygen values (New-
490 Zealand, $[O_2]$ ~> 250 mmol/m3). One site in the Neotethys doesn't follow this trend with data
491 documenting anoxic conditions at the location of which the model simulates elevated oxygen
492 concentrations (Fig.11). This inconsistency could be due to the complex paleogeography of
493 the western Neotethys that is compartmented in numerous restricted deep basins separated by
494 shallow platforms (Golonka et al., 2000; Nouri et al., 2016). Anoxia could locally exist in
495 such basins but this degree of complexity is not represented at the spatial resolution of our
496 model.
497 Seafloor oxygen concentrations in the Central Atlantic basin are, in contrast, highly
498 sensitive to the configuration of the CAS and a specific comparison to data is made in section
499 4.3 for the Central Atlantic. For areas where the oxygen level is relatively insensitive to CAS
500 depths, i.e. the southern Central Atlantic and the northern Gulf of Mexico, the model
501 reproduces the dysoxic and anoxic areas inferred from proxy data for the pre-OAE2 interval
502 (Figs. 10 and 11a). Finally, the WIS represents another location of model-data mismatch in
503 the three simulations because the model suggests oxygenated conditions at odds with
504 observations of anoxia at this site (2 dots, see Fig.11a). However, the oxygenation state has
505 been shown to be related to sea-level variations in this region (Lowery et al., 2018), which are
506 not taken into account in the simulations and may provide an explanation to the model/data
507 discrepancy.
508 At the global scale, the spatial patterns of simulated seafloor oxygen are consistent
509 with the modelling study of Monteiro et al. (2012) that uses the GENIE EMIC. The most
510 severe anoxic regions are the Central/Equatorial Atlantic and dysoxia is simulated in the
511 Neotethys and Eastern Pacific oceans whereas the Southern Pacific remains more oxygenated.
512 The seafloor is however globally less oxygenated in Monteiro et al. (2012), likely due to a
513 less intense overturning circulation (around 6 Sv in the intermediate ocean vs. 18 Sv in our
514 study). Another major difference is observed in the South Atlantic where the model of
515 Monteiro et al. (2012) simulates higher oxygen concentrations, probably due to deep-water
516 formation in this area, which is absent in our model. This inconsistency is hard to resolve at
517 the moment as there is no data available in this region for the Cenomanian. From a physical

perspective, Donnadieu et al. (2016) also suggested weak deep-water formation in the South Atlantic using the coarse-resolution FOAM global climate model. On the contrary, the more complex CCSM4 ESM Cenomanian simulation of Ladant et al. (2020) does not produce deep-water formation in the South Atlantic, indicating that these inconsistencies could be a problem of model complexity and resolution, and/or employed paleogeography.

Our results illustrate a long-term control of paleogeography on oceanic oxygen beyond OAE2 shorter-term triggers. For example, the anoxia located in the Southern Central and Equatorial Atlantic is a robust feature of our and previous simulations (Monteiro et al. 2012) under pre-OAE2 conditions and is also inferred from pre-OAE2 data, suggesting that this localized anoxia is driven by paleogeography and is decoupled from the specific triggers of the OAE2. In addition, regions where anoxia spreads over during OAE2 were those already characterized by reduced oxygenation in our model. Our results therefore suggest a significant preconditioning of the global ocean oxygenation on the runup to the OAE2 driven by paleogeographic setting of the Cenomanian. More generally, we can hypothesize that ocean preconditioning is required for OAEs to occur (See also Song et al., 2019) and that shorter-term controllers (such as an abrupt rise of pCO_2 or an increase in nutrient supply) would then turn preconditioned areas into hypoxic or anoxic environments (See also Dummann et al., 2020a).

1.2 Constraining Oceanic Gateways paleobathymetry.

The CLIP is estimated to have mainly formed between 95 and 83 Ma in the Pacific Ocean westward of the CAS and to have moved through the CAS during the Late Cretaceous (Andjić et al., 2019; Dürkefälden et al., 2019; Loewen et al., 2013; Romito & Mann, 2020), thereby shallowing the connection between the Central Atlantic and Pacific oceans (Buchs et al., 2018). Numerous evidence suggest a significant role for the CLIP volcanism in the initiation of OAE2 (Joo et al., 2020; Kerr & Kerr, 1998; Turgeon & Creaser, 2008). However, the timing of its formation and progressive eastward movement is not well constrained. This complexity limits inferences about the potential contribution of a CLIP-induced shallowing of the CAS to OAE2. In an attempt to better constrain the CAS paleobathymetry during the Late Cenomanian, we compare the study sites of the Central Atlantic to our three scenarios of seafloor oxygen simulated for the different CAS configurations (Deep, Intermediate, Shallow; Fig.10).

Seven sites document anoxic conditions before OAE2. They are located in the Southern Central Atlantic and in the Gulf of Mexico (Fig 10; Perez-Infante et al., 1996; Kuypers et al., 2002; Owens et al., 2012; van Helmond et al., 2014b; Westermann et al., 2014; Lowery et al., 2017). In particular, previous studies suggested that the anoxic area surrounding the Equatorial Atlantic Gateway was driven by the estuarine circulation established between the Pacific and Central Atlantic (Topper et al., 2011; Trabucho Alexandre et al., 2010) but our results demonstrate that this anoxic area is stable even in the *ShallowCAS* simulation despite the disappearance of the estuarine circulation. Our findings imply that this anoxic zone would rather be driven by the global paleogeography than regionally controlled by the CAS. In fact, all these pre-OAE2 anoxic sites are located in regions simulated as hypoxic to anoxic regardless of the CAS configuration and, thus, a comparison between our simulations does not help constraining the CAS depth.

In the deep Central Atlantic, five sites record oxic conditions before OAE2 (Fig. 10; Owens et al., 2012; van Helmond et al., 2014b). The comparison with modelling results is partially consistent only for the *DeepCAS* simulation (Fig. 10a). In this scenario, the deep connection (> 2500 meters depth) between the Pacific and Central Atlantic basins allows oxygenated deep waters from the Pacific to flow into and fill the western part of the deep Central Atlantic (Supplementary Fig.S8), resulting in simulated oxic deep waters that correlate with the proxy record. In the *IntermediateCAS* simulation, the shallower CAS (< 2500 meters of water depth) prevents these oxygenated deep waters to penetrate into the Central Atlantic, which is supplied by oxygen-poor intermediate waters resulting in hypoxic conditions, which is not consistent with data in the deep Central Atlantic for the pre-OAE2 (Fig. 10b). The same conclusion is made for the *ShallowCAS* scenario, for which the deep Central Atlantic is fully anoxic due to very high sea-bottom temperature and subsidence of anoxic waters from the Equatorial Atlantic Gateway (Fig. 10c).

Our numerical results thus suggest that a CAS opened only to upper ocean circulation is unlikely in the Cenomanian because a long-term complete anoxia does not characterize the Central Atlantic basin besides during the OAE2. Our simulations underline that deep connections are required between the two basins prior to the OAE2 in order to fill the Central Atlantic with well-oxygenated deep waters. This result suggests either a motion of the CLIP through the CAS coeval, at the earliest, with the beginning of the OAE2, or the existence of multiple volcanic arc systems separated by deep channels around the CLIP (Romito & Mann, 2020). A tantalizing implication of our results is that the early eastward movement of the CLIP across the CAS at the end of the Cenomanian may have participated in the formation of

a complete anoxia in the deep Central Atlantic during the OAE2. The transition from abyssal (4000 m, the DeepCAS) to bathyal depths (2500 m, IntermediateCAS) in our simulations indeed contribute to decreasing seafloor oxygen concentrations in the Central Atlantic. However supplementary simulations are needed to corroborate this hypothesis as other factors, such as an enhanced supply of nutrients to the ocean consecutive to volcanism or pCO2 increase (Adams et al., 2010; Barclay et al., 2010; Joo et al., 2020; Pogge Von Strandmann et al., 2013; Turgeon & Creaser, 2008) may force the deep Central Atlantic to become anoxic despite deep ocean connections across the CAS.

The eastern part of the Central Atlantic remains hypoxic to anoxic in the deep, regardless of the CAS depth, probably because of the combination of its bottleneck configuration for deep circulation and of elevated marine productivity above (Supplementary Fig.S6). These reduced oxygen conditions are inconsistent with pre-OAE2 data for the eastern Central Atlantic that document oxic environments (Niels A. G. M. van Helmond et al., 2014). This discrepancy suggests that an intermittent source of oxygenated deep waters may have existed in the northern part of the Cenomanian Central Atlantic, thereby creating oxic conditions in the deep eastern side of the basin (Fig. 10; Sites 1276 and 641) prior to the OAE2 and also providing an explanation to the temporary re-oxygenation of the deep Central Atlantic during the Plenus Cold Event within the OAE2 (van Helmond et al. 2014b). The recent Cenomanian simulation of Ladant et al. (2020) indicate possible deep-water formation in the Cenomanian North Atlantic but this source does not exist in our simulations, and we note that evidence is lacking to unambiguously confirm its existence. A deeper connection with the Neotethys is also suggested during the Late Cretaceous (Buchs et al., 2018; Nouri et al., 2016) and could supply oxygen to the North-Eastern Central Atlantic. However, reconstructing paleogeography and paleobathymetry in this area is particularly challenging because the Neotethyan region is composed of numerous shallow carbonate platforms separated by deep and narrow corridors (Stampfli and Borel 2002). As such, we cannot draw from our results anything but speculative conclusions about a possible role of the Tethys Seaway on the evolution of deep Central Atlantic oxygenation.

1.3 How to make anoxic an ocean despite an active circulation?

Very weak renewal of deep-water masses is often needed to generate anoxia in an ocean basin. Silled basins are a prime example as they are affected by a strong circulation restriction and stratification with long water renewal rate (Algeo & Lyons, 2006). It was for instance calculated that the renewal rate in the anoxic Cleveland basin during the Toarcian Oceanic

Anoxic Event was between 4000 and 40 000 years (McArthur et al., 2008). During the OAE2, the renewal rate in the deep Central Atlantic is estimated between 500 and 4000 years (Niels A. G. M. van Helmond et al., 2014), which is similar to that of the modern Black Sea (Algeo & Lyons, 2006). This estimation is consistent with the three simulated scenarios that exhibit water ages in the deep Central Atlantic comprised between ~500 years (in the *ShallowCAS* simulation) and ~2000 years (in the *IntermediateCAS* simulation). The ShallowCAS scenario provides interesting insights in terms of ocean dynamics and oxygenation mechanisms by showing that the degree of oxygen depletion can be linked to the provenance of water masses rather than a sluggish circulation. Indeed, this silled basin in the ShallowCAS simulation exhibits an active deep circulation (around 5-6 Sv), with relatively short renewal age, and is fully anoxic at the same time because incoming subsiding waters that flow into the deep Central Atlantic come from the anoxic OMZ of the Equatorial Atlantic Gateway. These results propose an alternative to the common view that ocean stagnation is required to create anoxia and enhance organic carbon burial in deep basins.

Previous model studies have also suggested that ocean stagnation was not sufficient to create intermediate to shallow anoxia/euxinia (Ozaki et al. 2011, Monteiro et al. 2012). (Ozaki et al., 2011) showed that ocean stagnation only promoted deep-water anoxia and that massive phosphorus inputs were additionally required to create a global anoxia by enhancement of marine productivity. Monteiro et al. (2012) observed as well that enhanced marine productivity due to higher nutrient content was the most efficient process to expand oceanic anoxia. In contrast, our findings demonstrate that full basin-scale anoxia can co-exist with an active ocean circulation and without the need for enhanced productivity.

5. Conclusion

The activity of the CLIP in the Late Cenomanian have impacted the paleobathymetry of the CAS via the formation of the Caribbean plateau. In this study, we use the IPSLCM5A2 earth system model, which includes the marine biogeochemistry model PISCES, to explore the impact of the paleobathymetry of the CAS on oceanic circulation and dissolved oxygen distribution during the Cenomanian. Regardless of the depth of the CAS, the model simulates an active oceanic circulation, dominated by the Pacific Ocean. The spatial variations of the global oxygen distribution compare well with pre-OAE2 proxy records and exhibit oceanic environments ranging from fully oxic to fully anoxic. These spatial variations are strongly driven by the global paleobathymetry and by the configuration of oceanic gateways that

control the pathways of deep currents and the associated oxygen supply. Restricted basins such as the Central and South Atlantic are oxygen-poor and even locally anoxic in all simulations, while the deep Southern Pacific is well-oxygenated because it is a region of deep-water formation. The depth of the CAS, however, exerts substantial control on the seafloor oxygen concentration of the Central Atlantic basin. In the DeepCAS configuration, most of the deep western Central Atlantic is oxic whereas the deep eastern part of the basin is dysoxic. Dysoxia spreads westward in the IntermediateCAS configuration while a complete anoxia develops in the whole basin in the ShallowCAS configuration. A comparison with redox proxy data suggests that a deep connection (> 2500 meters) existed before the OAE2 between the Pacific and Central Atlantic. A shallowing of the CAS to an intermediate depth (~2500 meters of water depth) due to the eastward movement of the Caribbean LIP may have participated in the establishment of complete hypoxic to anoxic environments in the deep Central Atlantic, by reducing the oxygen supply from Pacific bottom waters. These results illustrate how long-term paleobathymetric forcings may precondition the ocean for favorable low-oxygen conditions allowing OAEs to develop and high quantity of organic carbon to be preserved in the oceans and eventually buried.

DATA AVAILABILITY STATEMENT

Code availability:
LMDZ, XIOS, NEMO and ORCHIDEE are released under the terms of the CeCILL license. OASIS-MCT is released under the terms of the Lesser GNU General Public License (LGPL). IPSL-CM5A2 code is publicly available through svn, with the following command lines: svn co http://forge.ipsl.jussieu.fr/igcmg/svn/modipsl/branches/publications/IPSLCM5A2.1_11192019 modipsl
cd modipsl/util;./model IPSLCM5A2.1
The mod.def file provides information regarding the different revisions used, namely:
– NEMOGCM branch nemo_v3_6_STABLE revision 6665
– XIOS2 branchs/xios-2.5 revision 1763
– IOIPSL/src svn tags/v2_2_2
– LMDZ5 branches/IPSLCM5A2.1 rev 3591
– branches/publications/ORCHIDEE_IPSLCM5A2.1.r5307 rev 6336
– OASIS3-MCT 2.0_branch (rev 4775 IPSL server)
The login/password combination requested at first use to download the ORCHIDEE component is anonymous/anonymous. We recommend to refer to the project website: http://forge.ipsl.jussieu.fr/igcmg_doc/wiki/Doc/Config/IPSLCM5A2 for a proper installation and compilation of the environment.

Data availability: Datasets from previously published sources have been used for this research. The complete list of references is detailed in the Supporting Data D1.

AKNOWLEDGMENTS

We express our thanks to Total E&P for funding the project and granting permission to publish. We acknowledge Olivier Aumont for their contribution to the development of the adapted version of the PISCES code for deep-time simulations. We thank the CEA/CCRT for providing access to the HPC resources of TGCC under the allocation 2017-A0010102212, 2018-A0030102212, and 2019-A0050102212 made by GENCI. We acknowledge the use of Ferret (ferret.pmel.noaa.gov/Ferret/), NCL and ArcGIS softwares for analysis and figures in this paper.

REFERENCES

Adams, D. D., Hurtgen, M. T., & Sageman, B. B. (2010). Volcanic triggering of a biogeochemical cascade during Oceanic Anoxic Event 2. *Nature Geoscience*, *3*(3), 201–204. https://doi.org/10.1038/ngeo743

Algeo, T. J., & Lyons, T. W. (2006). Mo-total organic carbon covariation in modern anoxic marine environments: Implications for analysis of paleoredox and paleohydrographic conditions. *Paleoceanography*, *21*(1). https://doi.org/10.1029/2004PA001112

Andjić, G., Baumgartner, P. O., & Baumgartner-Mora, C. (2019). Collision of the Caribbean Large Igneous Province with the Americas: Earliest evidence from the forearc of Costa Rica. *Bulletin of the Geological Society of America*, *131*(9–10), 1555–1580. https://doi.org/10.1130/B35037.1

Arthur, M. A., Schlanger, S. O., & Jenkyns, H. C. (1987). The Cenomanian-Turonian Oceanic Anoxic Event , II . Palaeoceanographic controls on organic-matter production and preservation Timing of Cenomanian-Turonian events and the duration of the, (26), 401–420.

Aumont, O., Ethé, C., Tagliabue, A., Bopp, L., & Gehlen, M. (2015). PISCES-v2: An ocean biogeochemical model for carbon and ecosystem studies. *Geoscientific Model Development*, *8*(8), 2465–2513. https://doi.org/10.5194/gmd-8-2465-2015

Barclay, R. S., McElwain, J. C., & Sageman, B. B. (2010). Carbon sequestration activated by a volcanic CO 2 pulse during Ocean Anoxic Event 2. *Nature Geoscience*, *3*(3), 205–208. https://doi.org/10.1038/ngeo757

Batenburg, S. J., De Vleeschouwer, D., Sprovieri, M., Hilgen, F. J., Gale, A. S., Singer, B. S., et al. (2016). Orbital control on the timing of oceanic anoxia in the Late Cretaceous. *Climate of the Past*, *12*(10), 2009–2016. https://doi.org/10.5194/cp-12-1995-2016

Bice, K. L., Birgel, D., Meyers, P. A., Dahl, K. A., Hinrichs, K. U., & Norris, R. D. (2006). A multiple proxy and model study of Cretaceous upper ocean temperatures and atmospheric CO2 concentrations. *Paleoceanography*, *21*(2), 1–17. https://doi.org/10.1029/2005PA001203

Blättler, C. L., Jenkyns, H. C., Reynard, L. M., & Henderson, G. M. (2011). Significant increases in global weathering during Oceanic Anoxic Events 1a and 2 indicated by calcium isotopes. *Earth and Planetary Science Letters*, *309*(1–2), 77–88. https://doi.org/10.1016/j.epsl.2011.06.029

Bopp, L., Resplandy, L., Untersee, A., Le Mezo, P., & Kageyama, M. (2017). Ocean (de)oxygenation from the Last Glacial Maximum to the twenty-first century: Insights from Earth System models. *Philosophical Transactions of the Royal Society A: Mathematical, Physical and Engineering Sciences*, *375*(2102). https://doi.org/10.1098/rsta.2016.0323

Buchs, D. M., Kerr, A. C., Brims, J. C., Zapata-Villada, J. P., Correa-Restrepo, T., & Rodríguez, G. (2018). Evidence for subaerial development of the Caribbean oceanic plateau in the Late Cretaceous and palaeo-environmental implications. *Earth and Planetary Science Letters*, *499*, 62–73. https://doi.org/10.1016/j.epsl.2018.07.020

Degens, E. T., & Stoffers, P. (1976). Stratified waters as a key to the past. *Nature*, *263*(5572), 22–27. https://doi.org/10.1038/263022a0

Donnadieu, Y., Pierrehumbert, R., Jacob, R., & Fluteau, F. (2006). Modelling the primary control of paleogeography on Cretaceous climate. *Earth and Planetary Science Letters*, *248*(1–2), 411–422. https://doi.org/10.1016/j.epsl.2006.06.007

Donnadieu, Yannick, Pucéat, E., Moiroud, M., Guillocheau, F., & Deconinck, J. F. (2016). A better-ventilated ocean triggered by Late Cretaceous changes in continental configuration. *Nature Communications*, *7*. https://doi.org/10.1038/ncomms10316

Dufresne, J. L., Foujols, M. A., Denvil, S., Caubel, A., Marti, O., Aumont, O., et al. (2013). *Climate change projections using the IPSL-CM5 Earth System Model: From CMIP3 to CMIP5*. *Climate Dynamics* (Vol. 40). https://doi.org/10.1007/s00382-012-1636-1

Dummann, W., Steinig, S., Hofmann, P., Flögel, S., Osborne, A. H., Frank, M., et al. (2020). The impact of Early Cretaceous gateway evolution on ocean circulation and organic carbon burial in the emerging South Atlantic and Southern Ocean basins. *Earth and Planetary Science Letters*, *530*, 115890. https://doi.org/10.1016/j.epsl.2019.115890

Dummann, Wolf, Steinig, S., Hofmann, P., Lenz, M., Kusch, S., Herrle, J. O., et al. (2020). Driving mechanisms of organic carbon burial in the Early Cretaceous South Atlantic Cape Basin (DSDP Site 361), (March), 1–30.

Dürkefälden, A., Hoernle, K., Hauff, F., Wartho, J. A., van den Bogaard, P., & Werner, R. (2019). Age and geochemistry of the

Beata Ridge: Primary formation during the main phase (~89 Ma) of the Caribbean Large Igneous Province. *Lithos*, *328–329*, 69–87. https://doi.org/10.1016/j.lithos.2018.12.021

Eldrett, J. S., Minisini, D., & Bergman, S. C. (2014). Decoupling of the carbon cycle during ocean anoxic event 2. *Geology*, *42*(7), 567–570. https://doi.org/10.1130/G35520.1

Erbacher, J., Huber, B. T., Norris, R. D., & Markey, M. (2001). Increased thermohaline stratification as a possible cause for an ocean anoxic event in the cretaceous period. *Nature*, *409*(6818), 325–327. https://doi.org/10.1038/35053041

Fichefet, T., & Maqueda, M. A. M. (1997). Sensitivity of a global sea ice model to the treatment of ice thermodynamics and dynamics. *Journal of Geophysical Research: Oceans*, *102*(C6), 12609–12646. https://doi.org/10.1029/97JC00480

Flögel, S., Wallmann, K., Poulsen, C. J., Zhou, J., Oschlies, A., Voigt, S., & Kuhnt, W. (2011). Simulating the biogeochemical effects of volcanic CO2degassing on the oxygen-state of the deep ocean during the Cenomanian/Turonian Anoxic Event (OAE2). *Earth and Planetary Science Letters*, *305*(3–4), 371–384. https://doi.org/10.1016/j.epsl.2011.03.018

Gangl, S. K., Moy, C. M., Stirling, C. H., Jenkyns, H. C., Crampton, J. S., Clarkson, M. O., et al. (2019). High-resolution records of Oceanic Anoxic Event 2: Insights into the timing, duration and extent of environmental perturbations from the palaeo-South Pacific Ocean. *Earth and Planetary Science Letters*, *518*, 172–182. https://doi.org/10.1016/j.epsl.2019.04.028

Gernigon, L., Franke, D., Geoffroy, L., Schiffer, C., Foulger, G. R., & Stoker, M. (2020). Crustal fragmentation, magmatism, and the diachronous opening of the Norwegian-Greenland Sea. *Earth-Science Reviews*, *206*(December 2018). https://doi.org/10.1016/j.earscirev.2019.04.011

Golonka, J., Oszczypko, N., & Ślączka, A. (2000). Late Carboniferous Neogene geodynamic evolution and palaeogeography of the circum-Carpathian region and adjacent areas. *Annales Societatis Geologorum Poloniae*.

Gough. (1981). Solar interior structure variations*. *Solar Physics*, *74*(September 1980), 21–34.

Van Helmond, N. A.G.M., Sluijs, A., Sinninghe Damsté, J. S., Reichart, G. J., Voigt, S., Erbacher, J., et al. (2015). Freshwater discharge controlled deposition of Cenomanian-Turonian black shales on the NW European epicontinental shelf (Wunstorf, northern Germany). *Climate of the Past*, *11*(3), 495–508. https://doi.org/10.5194/cp-11-495-2015

van Helmond, Niels A. G. M., Ruvalcaba Baroni, I., Sluijs, A., Sinninghe Damsté, J. S., & Slomp, C. P. (2014). Spatial extent and degree of oxygen depletion in the deep proto-North Atlantic basin during Oceanic Anoxic Event 2. *Geochemistry, Geophysics, Geosystems*, *15*(11), 4254–4266. https://doi.org/10.1002/2014GC005528

van Helmond, Niels A.G.M., Sluijs, A., Reichart, G. J., Damstï¿½, J. S. S., Slomp, C. P., & Brinkhuis, H. (2014). A perturbed hydrological cycle during Oceanic Anoxic Event 2. *Geology*, *42*(2), 123–126. https://doi.org/10.1130/G34929.1

Hourdin, F., Foujols, M. A., Codron, F., Guemas, V., Dufresne, J. L., Bony, S., et al. (2013). Impact of the LMDZ atmospheric grid configuration on the climate and sensitivity of the IPSL-CM5A coupled model. *Climate Dynamics*, *40*(9–10), 2167–2192. https://doi.org/10.1007/s00382-012-1411-3

Jenkyns, H. C. (2010). Geochemistry of oceanic anoxic events. *Geochemistry, Geophysics, Geosystems*, *11*(3), 1–30. https://doi.org/10.1029/2009GC002788

Jenkyns, H. C., Dickson, A. J., Ruhl, M., & van den Boorn, S. H. J. M. (2017). Basalt-seawater interaction, the Plenus Cold Event, enhanced weathering and geochemical change: deconstructing Oceanic Anoxic Event 2 (Cenomanian–Turonian, Late Cretaceous). *Sedimentology*, *64*(1), 16–43. https://doi.org/10.1111/sed.12305

Jones, M. M., Sageman, B. B., Oakes, R. L., Parker, A. L., Leckie, R. M., Bralower, T. J., et al. (2019). Astronomical pacing of relative sea level during Oceanic Anoxic Event 2: Preliminary studies of the expanded SH#1 Core, Utah, USA. *Bulletin of the Geological Society of America*, *131*(9–10), 1702–1722. https://doi.org/10.1130/B32057.1

Joo, Y. J., Sageman, B. B., & Hurtgen, M. T. (2020). Data-model comparison reveals key environmental changes leading to Cenomanian-Turonian Oceanic Anoxic Event 2. *Earth-Science Reviews*, *203*(February), 103123. https://doi.org/10.1016/j.earscirev.2020.103123

Kerr, A. C., & Kerr, A. C. (1998). Oceanic plateau formation : A cause of mass extinction and black shale deposition around the Cenomanian-Turonian boundary ? Oceanic plateau formation : a cause of mass extinction and black shale deposition around the Cenomanian – Turonian boundary ?, (May). https://doi.org/10.1144/gsjgs.155.4.0619

Krinner, G., Viovy, N., de Noblet-Ducoudré, N., Ogée, J., Polcher, J., Friedlingstein, P., et al. (2005). A dynamic global vegetation model for studies of the coupled atmosphere-biosphere system. *Global Biogeochemical Cycles*, *19*(1), 1–33. https://doi.org/10.1029/2003GB002199

Kuypers, M. M. M., Pancost, R. D., Nijenhuis, I. A., & Sinninghe Damsté, J. S. (2002). Enhanced productivity led to increased organic carbon burial in the euxinic North Atlantic basin during the late Cenomanian oceanic anoxic event. *Paleoceanography*, *17*(4), 3-1-3–13. https://doi.org/10.1029/2000PA000569

Ladant, J. B., Poulsen, C. J., Fluteau, F., Tabor, C. R., Macleod, K. G., Martin, E. E., et al. (2020). Paleogeographic controls on the evolution of Late Cretaceous ocean circulation. *Climate of the Past*, *16*(3), 973–1006. https://doi.org/10.5194/cp-16-973-2020

Laugié, M., Donnadieu, Y., Ladant, J., Green, J. A. M., & Bopp, L. (2020). Stripping back the modern to reveal the Cenomanian – Turonian climate and temperature gradient underneath, *2*, 953–971.

Li, Y. X., Montañez, I. P., Liu, Z., & Ma, L. (2017). Astronomical constraints on global carbon-cycle perturbation during Oceanic Anoxic Event 2 (OAE2). *Earth and Planetary Science Letters*, *462*, 35–46. https://doi.org/10.1016/j.epsl.2017.01.007

Loewen, M. W., Duncan, R. A., Kent, A. J. R., & Krawl, K. (2013). Prolonged plume volcanism in the Caribbean Large Igneous Province: New insights from Curaçao and Haiti. *Geochemistry, Geophysics, Geosystems*, *14*(10), 4241–4259. https://doi.org/10.1002/ggge.20273

Lowery, C. M., Cunningham, R., Barrie, C. D., Bralower, T., & Snedden, J. W. (2017). The Northern Gulf of Mexico During OAE2 and the Relationship Between Water Depth and Black Shale Development. *Paleoceanography*, *32*(12), 1316–1335. https://doi.org/10.1002/2017PA003180

Lowery, C. M., Leckie, R. M., Bryant, R., Elderbak, K., Parker, A., Polyak, D. E., et al. (2018). The Late Cretaceous Western Interior Seaway as a model for oxygenation change in epicontinental restricted basins. *Earth-Science Reviews*, *177*(December 2017), 545–564. https://doi.org/10.1016/j.earscirev.2017.12.001

MacLeod, K. G., Martin, E. E., & Blair, S. W. (2008). Nd isotopic excursion across Cretaceous ocean anoxic event 2 (Cenomanian-Turonian) in the tropical North Atlantic. *Geology*, *36*(10), 811–814. https://doi.org/10.1130/G24999A.1

Madec, G., & Imbard, M. (1996). A global ocean mesh to overcome the North Pole singularity. *Climate Dynamics*, *12*(6), 381–388. https://doi.org/10.1007/BF00211684

Madec, G., & Team, and the N. (2016). NEMO Ocean Engine. 2016, (27), 1–332. Retrieved from http://www.nemo-ocean.eu/About-NEMO/Reference-manuals$%5C$npapers2://publication/uuid/73E7FF17-99BE-4B10-A823-0037C823EF6E

Martin, E. E., MacLeod, K. G., Jiménez Berrocoso, A., & Bourbon, E. (2012). Water mass circulation on Demerara Rise during the Late Cretaceous based on Nd isotopes. *Earth and Planetary Science Letters*, *327–328*, 111–120. https://doi.org/10.1016/j.epsl.2012.01.037

Martinson, V. S., Heller, P. L., & Frerichs, W. E. (1998). Distinguishing middle Late Cretaceous tectonic events from regional sea-level change using foraminiferal data from the U.S. Western Interior. *Bulletin of the Geological Society of America*, *110*(2), 259–268. https://doi.org/10.1130/0016-7606(1998)110<0259:DMLCTE>2.3.CO;2

McArthur, J. M., Algeo, T. J., Van De Schootbrugge, B., Li, Q., & Howarth, R. J. (2008). Basinal restriction, black shales, Re-Os dating, and the Early Toarcian (Jurassic) oceanic anoxic event. *Paleoceanography*, *23*(4), 1–22. https://doi.org/10.1029/2008PA001607

Mitchell, R. N., Bice, D. M., Montanari, A., Cleaveland, L. C., Christianson, K. T., Coccioni, R., & Hinnov, L. A. (2008). Oceanic anoxic cycles? Orbital prelude to the Bonarelli Level (OAE 2). *Earth and Planetary Science Letters*, *267*(1–2), 1–16. https://doi.org/10.1016/j.epsl.2007.11.026

Monteiro, F. M., Pancost, R. D., Ridgwell, A., & Donnadieu, Y. (2012). Nutrients as the dominant control on the spread of anoxia and euxinia across the Cenomanian-Turonian oceanic anoxic event (OAE2): Model-data comparison. *Paleoceanography*, *27*(4), 1–17. https://doi.org/10.1029/2012PA002351

Montoya-Pino, C., Weyer, S., Anbar, A. D., Pross, J., Oschmann, W., van de Schootbrugge, B., & Arz, H. W. (2010). Global enhancement of ocean anoxia during oceanic anoxic event 2: A quantitative approach using U isotopes. *Geology*, *38*(4), 315–318. https://doi.org/10.1130/G30652.1

Mourlot, Y., Roddaz, M., Dera, G., Calvès, G., Kim, J. H., Chaboureau, A. C., et al. (2018). Geochemical Evidence for Large-Scale Drainage Reorganization in Northwest Africa During the Cretaceous. *Geochemistry, Geophysics, Geosystems*, *19*(5), 1690–1712. https://doi.org/10.1029/2018GC007448

Müller, R. D., Sdrolias, M., Gaina, C., & Roest, W. R. (2008). Age, spreading rates, and spreading asymmetry of the world's ocean crust. *Geochemistry, Geophysics, Geosystems*, *9*(4), 1–19. https://doi.org/10.1029/2007GC001743

Nederbragt, a J., Thurow, J., Vonhof, H., & Brumsack, H. J. (2004). Modelling oceanic carbon and phosphorus fluxes: implications for the cause of the late Cenomanian Oceanic Anoxic Event (OAE2). *Journal of the Geological Society*, *161*(4), 721–728. https://doi.org/10.1144/0016-764903-075

Norris, R. D., Bice, K. L., Magno, E. A., & Wilson, P. A. (2002). Jiggling the tropical thermostat in the Cretaceous hothouse. *Geology*, *30*(4), 299–302. https://doi.org/10.1130/0091-7613(2002)030<0299:JTTTIT>2.0.CO;2

Nouri, F., Azizi, H., Golonka, J., Asahara, Y., Orihashi, Y., Yamamoto, K., et al. (2016). Age and petrogenesis of Na-rich felsic rocks in western Iran: Evidence for closure of the southern branch of the Neo-Tethys in the Late Cretaceous. *Tectonophysics*, *671*, 151–172. https://doi.org/10.1016/j.tecto.2015.12.014

O'Brien, C. L., Robinson, S. A., Pancost, R. D., Sinninghe Damsté, J. S., Schouten, S., Lunt, D. J., et al. (2017). Cretaceous sea-surface temperature evolution: Constraints from TEX 86 and planktonic foraminiferal oxygen isotopes. *Earth-Science Reviews*, *172*(March 2016), 224–247. https://doi.org/10.1016/j.earscirev.2017.07.012

Owens, J. D., Lyons, T. W., Li, X., MacLeod, K. G., Gordon, G., Kuypers, M. M. M., et al. (2012). Iron isotope and trace metal records of iron cycling in the proto-North Atlantic during the Cenomanian-Turonian oceanic anoxic event (OAE-2). *Paleoceanography*, *27*(3), 1–13. https://doi.org/10.1029/2012PA002328

Owens, J. D., Lyons, T. W., & Lowery, C. M. (2018). Quantifying the missing sink for global organic carbon burial during a Cretaceous oceanic anoxic event. *Earth and Planetary Science Letters*, *499*, 83–94. https://doi.org/10.1016/j.epsl.2018.07.021

Ozaki, K., Tajima, S., & Tajika, E. (2011). Conditions required for oceanic anoxia/euxinia: Constraints from a one-dimensional ocean biogeochemical cycle model. *Earth and Planetary Science Letters*, *304*(1–2), 270–279. https://doi.org/10.1016/j.epsl.2011.02.011

Perez-Infante, J., Farrimond, P., & Furrer, M. (1996). Global local controls influencing the deposition of the La Luna Formation (Cenomanian-Campanian), western Venezuela. *Chemical Geology*, *130*(3–4), 271–288. https://doi.org/10.1016/0009-2541(96)00019-8

Pogge Von Strandmann, P. A. E., Jenkyns, H. C., & Woodfine, R. G. (2013). Lithium isotope evidence for enhanced weathering during Oceanic Anoxic Event 2. *Nature Geoscience*, *6*(8), 668–672. https://doi.org/10.1038/ngeo1875

Poulsen, Chris J, Seidov, D., Barron, E. J., & Peterson, W. H. (1998). The impact of paleogeographic evolution on the surface oceanic circulation and the marine environment within the Mid-Cretaceous tethys, *13*(5), 546–559.

Poulsen, Christopher J., Barron, E. J., Arthur, M. A., & Peterson, W. H. (2001). Response of the mid-Cretaceous global oceanic circulation to tectonic and CO<inf>2</inf> forcings. *Paleoceanography*, *16*(6), 576–592. https://doi.org/10.1029/2000PA000579

Qin, X., Müller, R. D., Cannon, J., Landgrebe, T. C. W., Heine, C., Watson, R. J., & Turner, M. (2012). The GPlates Geological Information Model and Markup Language. *Geoscientific Instrumentation, Methods and Data Systems*, *1*(2), 111–134. https://doi.org/10.5194/gi-1-111-2012

Robinson, S. A., Dickson, A. J., Pain, A., Jenkyns, H. C., O'Brien, C. L., Farnsworth, A., & Lunt, D. J. (2019). Southern Hemisphere sea-surface temperatures during the Cenomanian-Turonian: Implications for the termination of Oceanic Anoxic Event 2. *Geology*, *47*(2), 131–134. https://doi.org/10.1130/G45842.1

Romito, S., & Mann, P. (2020). *Tectonic terranes underlying the present-day Caribbean plate: their tectonic origin, sedimentary thickness, subsidence histories and regional controls on hydrocarbon resources*. *Geological Society, London, Special Publications*. https://doi.org/10.1144/sp504-2019-221

Ruvalcaba Baroni, I., Topper, R. P. M., M. Van Helmond, N. A. G., Brinkhuis, H., & Slomp, C. P. (2014). Biogeochemistry of the North Atlantic during oceanic anoxic event 2: Role of changes in ocean circulation and phosphorus input. *Biogeosciences*, *11*(4), 977–993. https://doi.org/10.5194/bg-11-977-2014

Sageman, B. B., Meyers, S. R., & Arthur, M. A. (2006). Orbital time scale and new C-isotope record for Cenomanian-Turonian boundary stratotype. *Geology*, *34*(2), 125–128. https://doi.org/10.1130/G22074.1

Séférian, R., Gehlen, M., Bopp, L., Resplandy, L., Orr, J. C., Marti, O., et al. (2016). Inconsistent strategies to spin up models in CMIP5: Implications for ocean biogeochemical model performance assessment. *Geoscientific Model Development*, *9*(5), 1827–1851. https://doi.org/10.5194/gmd-9-1827-2016

Sepulchre, P., Caubel, A., Ladant, J. B., Bopp, L., Boucher, O., Braconnot, P., et al. (2020). IPSL-CM5A2 - An Earth system model designed for multi-millennial climate simulations. *Geoscientific Model Development*, *13*(7), 3011–3053. https://doi.org/10.5194/gmd-13-3011-2020

Sewall, J. O., Van De Wal, R. S. W., Van Der Zwan, K., Van Oosterhout, C., Dijkstra, H. A., & Scotese, C. R. (2007). Climate model boundary conditions for four Cretaceous time slices. *Climate of the Past*, *3*(4), 647–657. https://doi.org/10.5194/cp-3-647-2007

Sinninghe Damste, J. S., & Koster, J. (1998). A euxinic southern North Atlantic Ocean during the Cenomanian = Turonian oceanic anoxic event, *158*, 165–173.

Soares, D. M., Alves, T. M., & Terrinha, P. (2014). Contourite drifts on early passive margins as an indicator of established lithospheric breakup. *Earth and Planetary Science Letters*, *401*, 116–131. https://doi.org/10.1016/j.epsl.2014.06.001

Song, H., Wignall, P. B., Song, H., Dai, X., & Chu, D. (2019). Seawater Temperature and Dissolved Oxygen over the Past 500 Million Years. *Journal of Earth Science*, *30*(2), 236–243. https://doi.org/10.1007/s12583-018-1002-2

Tabor, C. R., Poulsen, C. J., Lunt, D. J., Rosenbloom, N. A., Otto-Bliesner, B. L., Markwick, P. J., et al. (2016). The cause of Late Cretaceous cooling: A multimodel-proxy comparison. *Geology*, *44*(11), 963–966. https://doi.org/10.1130/G38363.1

Talley, L. D., Reid, J. L., & Robbins, P. E. (2003). Data-Based Meridional Overturning Streamfunctions for the Global Ocean. *Journal of Climate*, *16*(19), 3213–3226. https://doi.org/10.1175/1520-0442(2003)016<3213:DMOSFT>2.0.CO;2

Thiéblemont, A., Hernández-Molina, F. J., Ponte, J. P., Robin, C., Guillocheau, F., Cazzola, C., & Raisson, F. (2020). Seismic stratigraphic framework and depositional history for Cretaceous and Cenozoic contourite depositional systems of the Mozambique Channel, SW Indian Ocean. *Marine Geology*, *425*(April), 106192. https://doi.org/10.1016/j.margeo.2020.106192

Topper, R. P. M., Trabucho Alexandre, J., Tuenter, E., & Meijer, P. T. (2011). A regional ocean circulation model for the mid-Cretaceous North Atlantic Basin: Implications for black shale formation. *Climate of the Past*, *7*(1), 277–297. https://doi.org/10.5194/cp-7-277-2011

Trabucho Alexandre, J., Tuenter, E., Henstra, G. A., Van Der Zwan, K. J., Van De Wal, R. S. W., Dijkstra, H. A., & De Boer, P. L. (2010). The mid-Cretaceous North Atlantic nutrient trap: Black shales and OAEs. *Paleoceanography*, *25*(4), 1–14. https://doi.org/10.1029/2010PA001925

Turgeon, S. C., & Creaser, R. A. (2008). Cretaceous oceanic anoxic event 2 triggered by a massive magmatic episode, *454*(July). https://doi.org/10.1038/nature07076

Valcke, S., Budich, R., Carter, M., Guilyardi, E., Lautenschlager, M., Redler, R., & Steenman-clark, L. (2006). The PRISM software framework and the OASIS coupler, *5*(September 2014), 2001–2004.

Du Vivier, A. D. C., Selby, D., Sageman, B. B., Jarvis, I., Gröcke, D. R., & Voigt, S. (2014). Marine187Os/188Os isotope stratigraphy reveals the interaction of volcanism and ocean circulation during Oceanic Anoxic Event 2. *Earth and Planetary Science Letters*, *389*, 23–33. https://doi.org/10.1016/j.epsl.2013.12.024

Wagner, T., Damste, J. S. S., Hofmann, P., & Beckmann, B. (2004). Euxinia and primary production in Late Cretaceous eastern equatorial Atlantic surface waters fostered orbitally driven formation of marine black shales, *19*(October), 1–13. https://doi.org/10.1029/2003PA000898

Wang, Y., Huang, C., Sun, B., Quan, C., Wu, J., & Lin, Z. (2014). Paleo-CO2 variation trends and the Cretaceous greenhouse climate. *Earth-Science Reviews*, *129*, 136–147. https://doi.org/10.1016/j.earscirev.2013.11.001

Wanninkhof, R. (1992). Relationship between wind speed and gas exchange over the ocean. *Journal of Geophysical Research*, *97*(C5), 7373–7382. https://doi.org/10.1029/92JC00188

Westermann, S., Vance, D., Cameron, V., Archer, C., & Robinson, S. A. (2014). Heterogeneous oxygenation states in the Atlantic and Tethys oceans during Oceanic Anoxic Event 2. *Earth and Planetary Science Letters*, *404*, 178–189. https://doi.org/10.1016/j.epsl.2014.07.018

Ye, J., Chardon, D., Rouby, D., Guillocheau, F., Dall'asta, M., Ferry, J. N., & Broucke, O. (2017). Paleogeographic and structural evolution of northwestern Africa and its Atlantic margins since the early Mesozoic. *Geosphere*, *13*(4), 1254–1284. https://doi.org/10.1130/GES01426.1

Zheng, X. Y., Jenkyns, H. C., Gale, A. S., Ward, D. J., & Henderson, G. M. (2013). Changing ocean circulation and hydrothermal inputs during Ocean Anoxic Event 2 (Cenomanian-Turonian): Evidence from Nd-isotopes in the European shelf sea. *Earth and Planetary Science Letters*, *375*, 338–348. https://doi.org/10.1016/j.epsl.2013.05.053

SUPPLEMENTARY INFORMATION

- Supporting Information S1
- Supporting Data D1

Figures

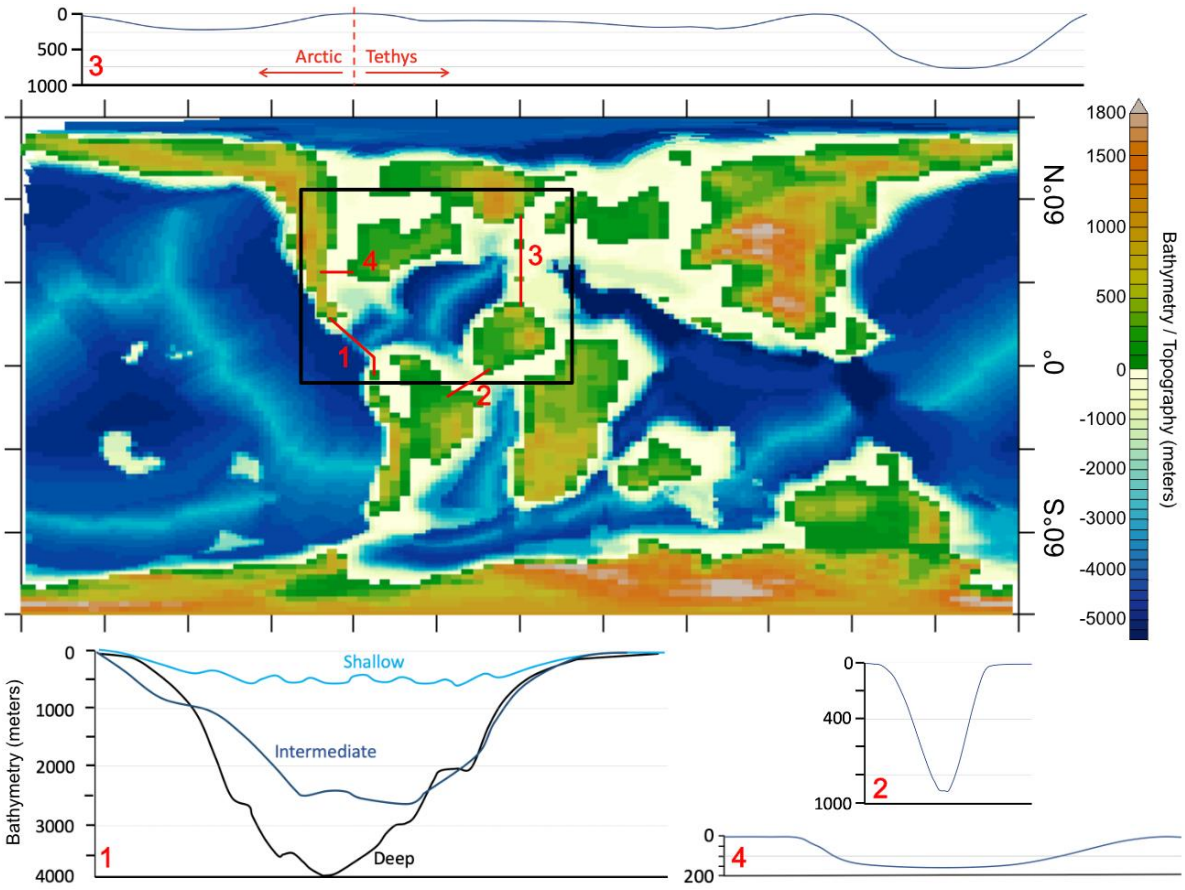

Figure 1: Cenomanian-Turonian paleogeographic configuration and bathymetric profiles of main gateways surrounding the Central Atlantic: (1) Central American Seaway (CAS). The three configurations correspond to different simulations. (2) Equatorial Atlantic Gateway (EAG). (3) Tethyan and Arctic seaways. (4) Western Interior Seaway (WIS). The black box corresponds to the region of interest of Figure 6.

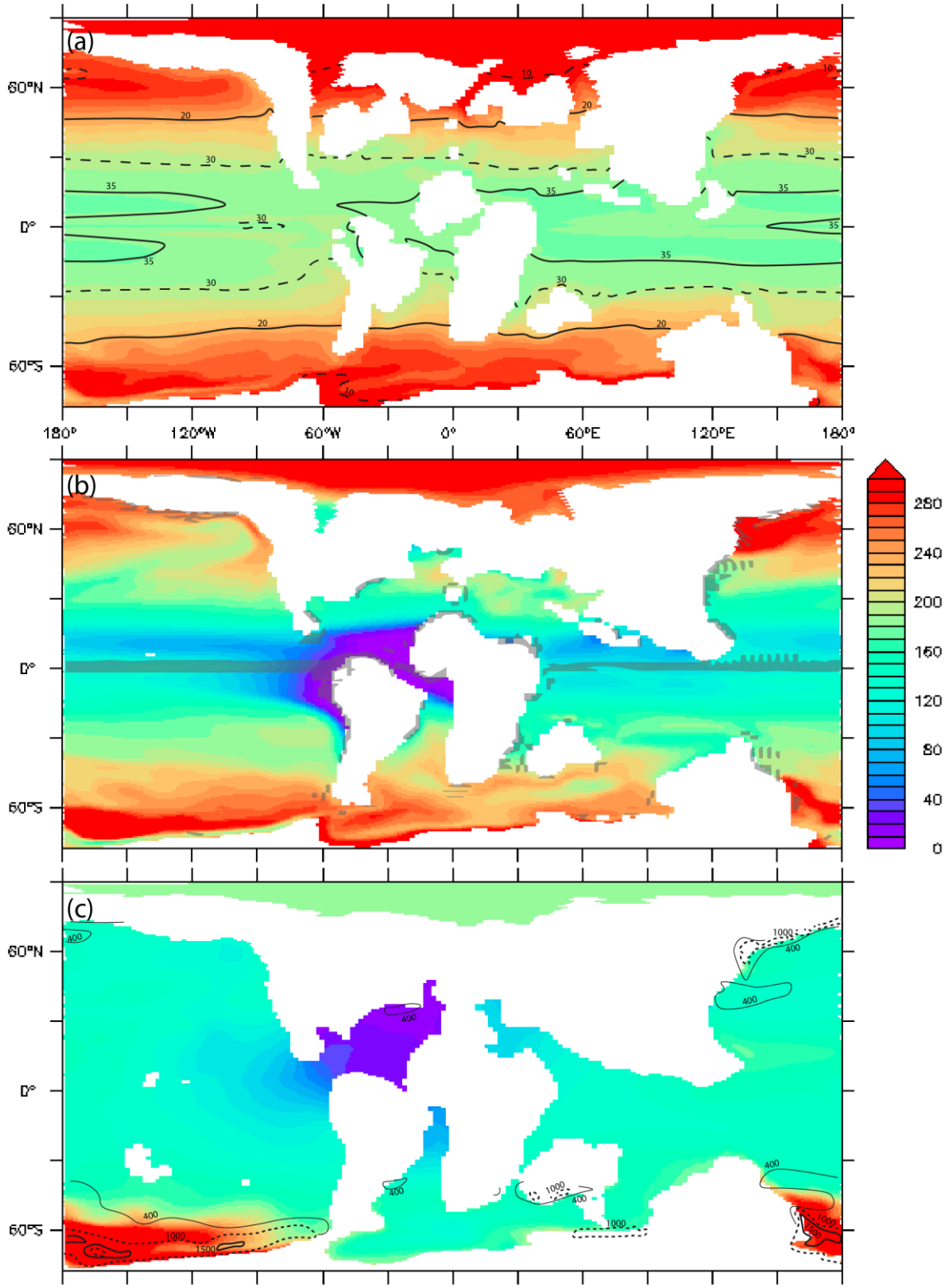

Figure 2: Oxygen concentration for the Deep CAS simulation (in mmol.m^{-3}); (a) At the surface level of the model (0-10 m) with contours of sea-surface temperatures (°C); (b) At 180 meters depth with areas of strong upwelling (grey shaded areas, vertical speed > 8 cm/day), and (c) At 700 meters depth with the mixed layer depth as contours (meters).

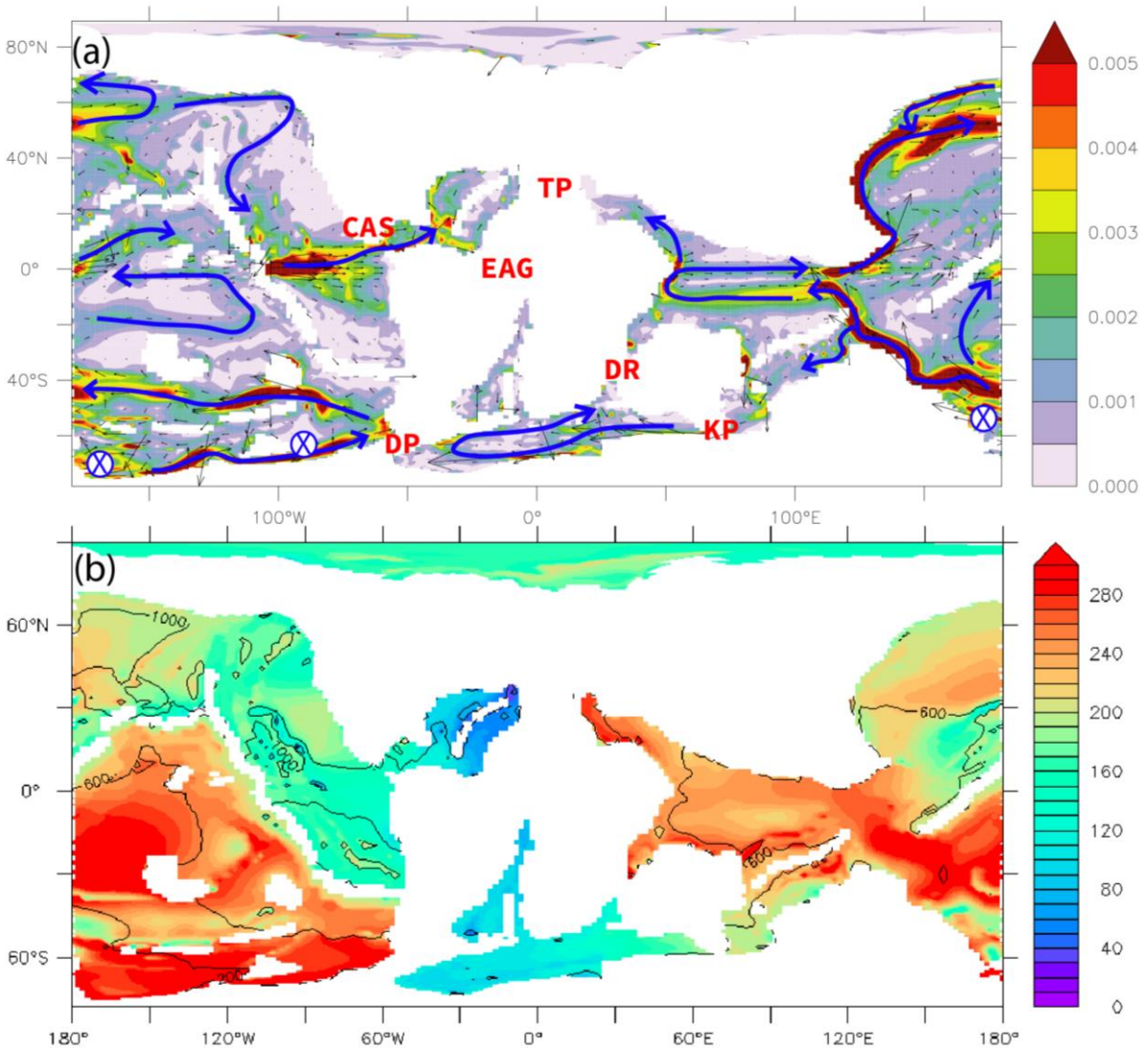

Figure 3: Oceanic circulation and oxygenation for the Deep CAS simulation. (a) Deep- currents velocity on the seafloor for areas where water depth > 3000 meters (m/s). Blue crosses correspond to areas of deep-water formation. Submarine topographic features are labelled in red: TP: Tethyan platforms, CAS: Central American Seaway, EAG: Equatorial Atlantic Gateway, DR: Davie Ridge, DP: Drake Passage, KP: Kerguelen Plateau. (b) Oxygen concentrations on the seafloor for areas where water depth > 3000 meters (mmol/m3). Black contours correspond to the water age at the same depth (years).

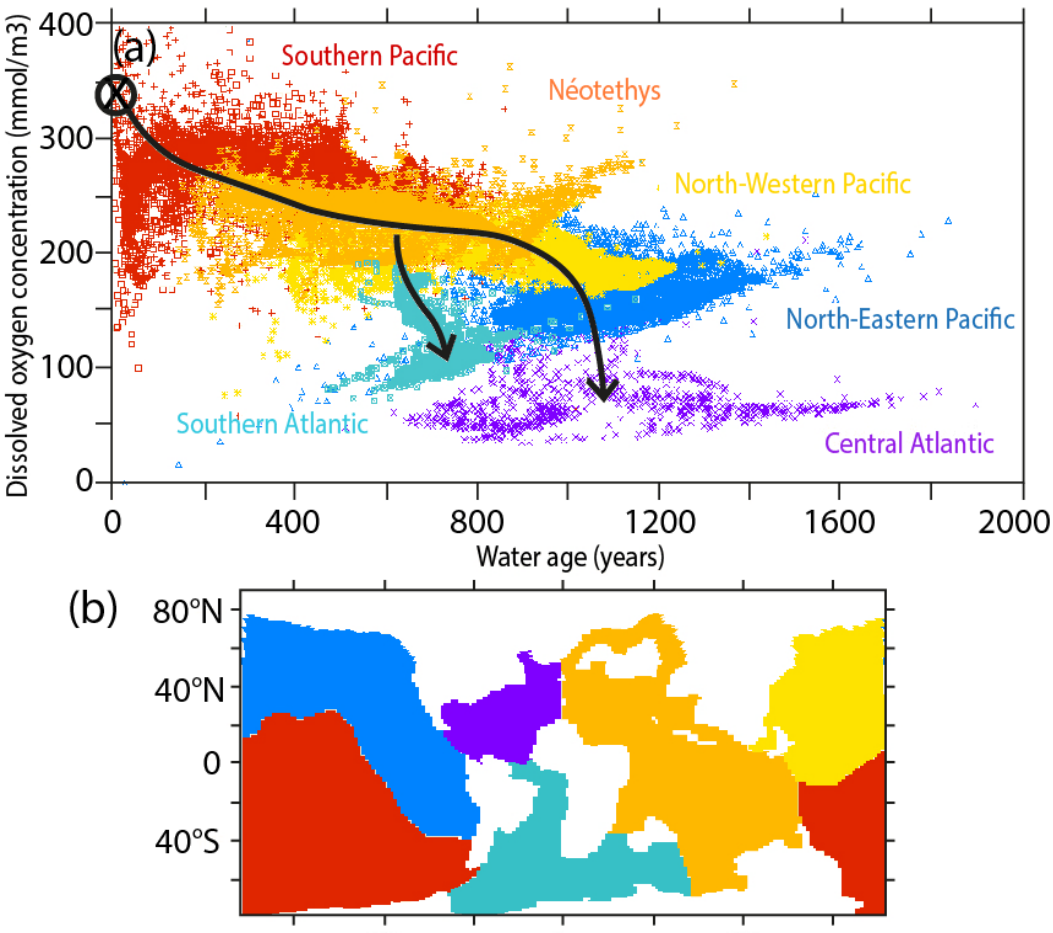

Figure 4: (a) Plot of water age (years) vs. oxygen concentration (mmol/m3) for water depth > 3000. Dots are colored by basin. Deep-water formation occurs in the Southern Pacific (Black cross) and black arrows indicate the two main circulation pathways through the basin. (b) Map showing the extent of different basins.

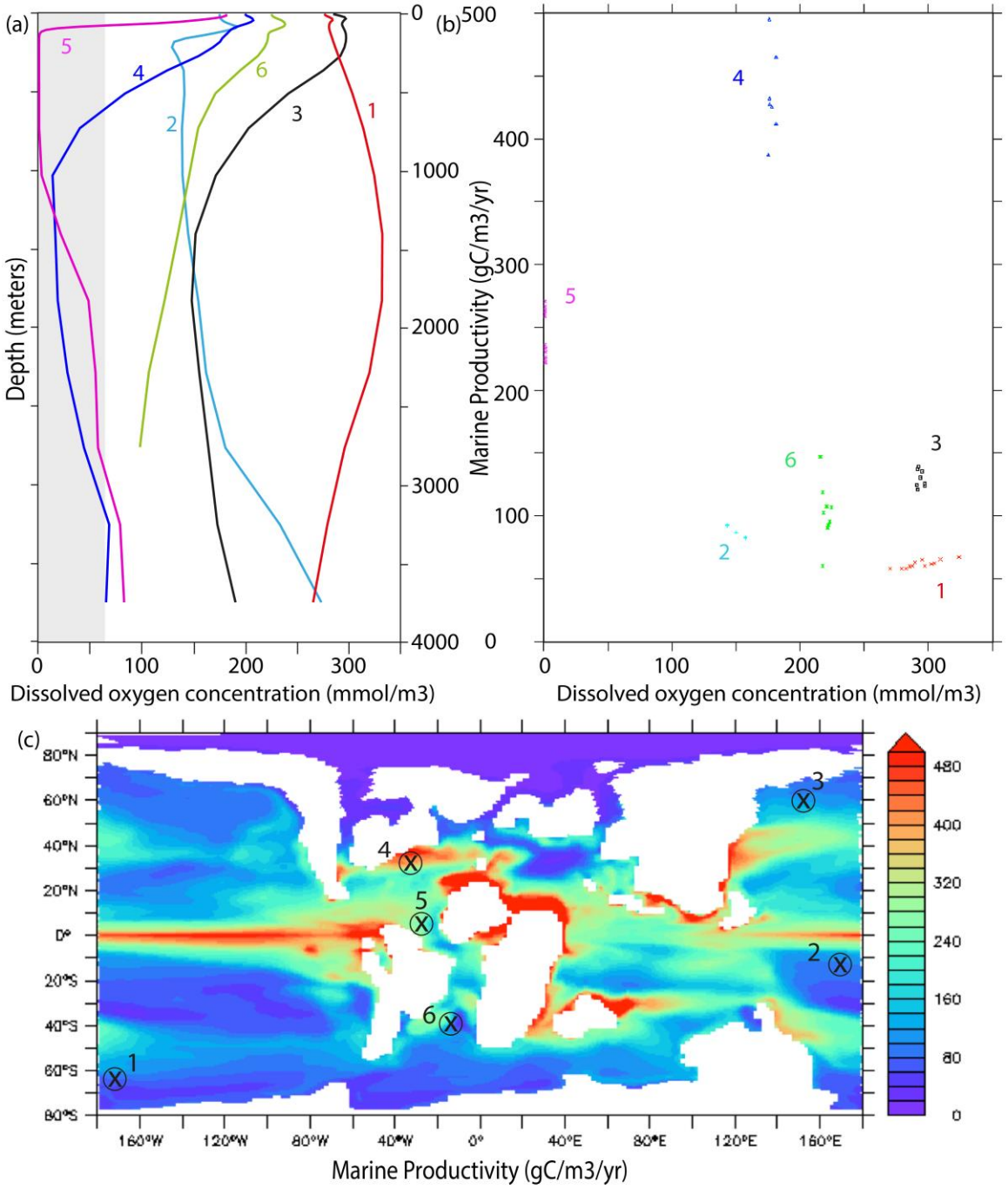

Figure5: (a) Vertical profiles in oxygen concentrations for the DeepCAS simulation. Locations are indicated on (c). (b) Marine productivity integrated over the whole water column ($gC.m^{-3}.yr^{-1}$) vs. oxygen concentration (integrated over the first 200 meters of water depth) plotted for locations around each profile of (a), covering -2/+2 decimal degrees in longitude and latitude around the profile. (c) Marine productivity integrated over the whole water column ($gC.m^{-3}.yr^{-1}$) and locations of profiles.

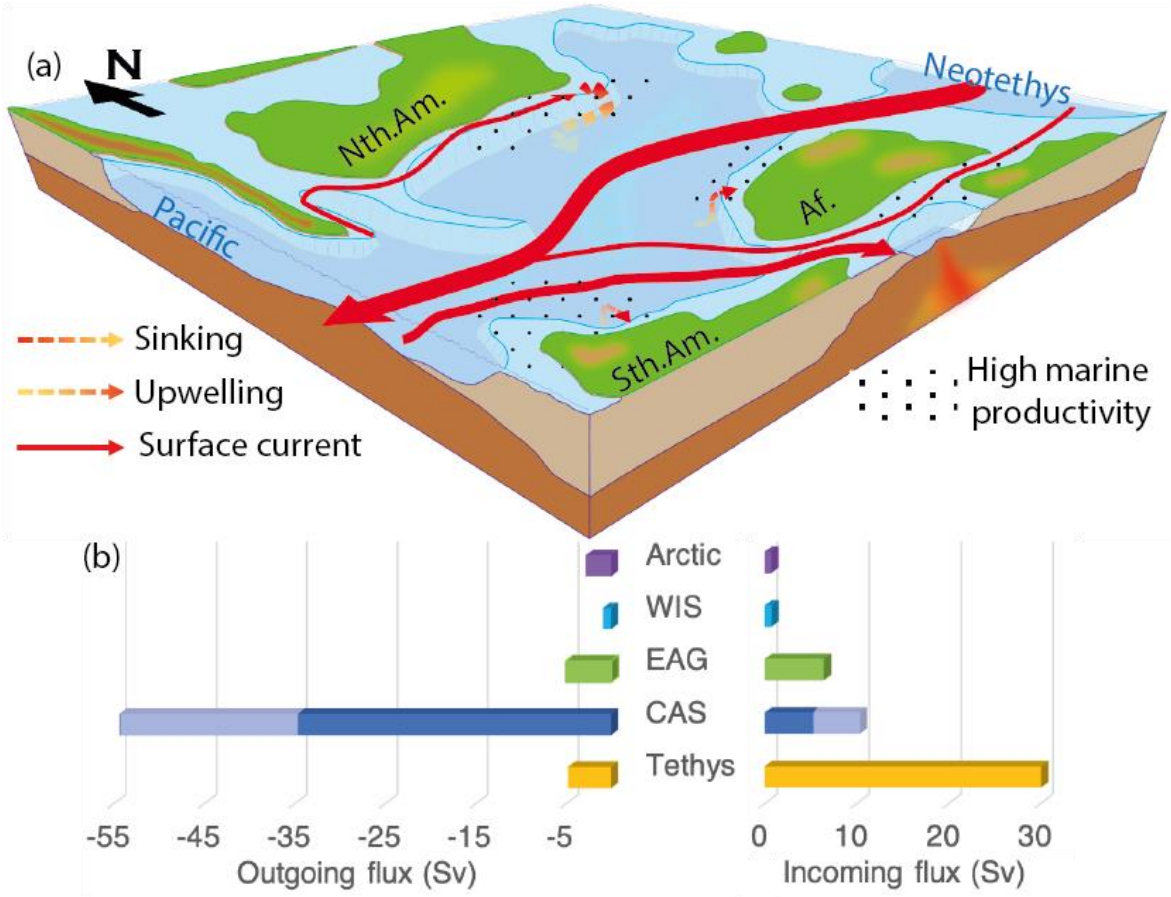

Figure 6: (a) Schematic representation of surface circulation in the Central Atlantic. See localization on Fig.1. Nth.Am.: North America, Sth.Am.: South America, Af.: Africa. (b) Incoming and outgoing fluxes (Sverdrups – Sv) into the Central Atlantic, computed through sections described in Fig.1. The histogram is calculated for the DeepCAS simulation, values for IntermediateCAS and ShallowCAS simulations are very similar, except for the incoming and outgoing fluxes through the CAS: the dark blue histogram corresponds to fluxes consistent in the three simulations, the shaded part of the histogram corresponds to supplementary fluxes observed only in IntermediateCAS and DeepCAS simulations.

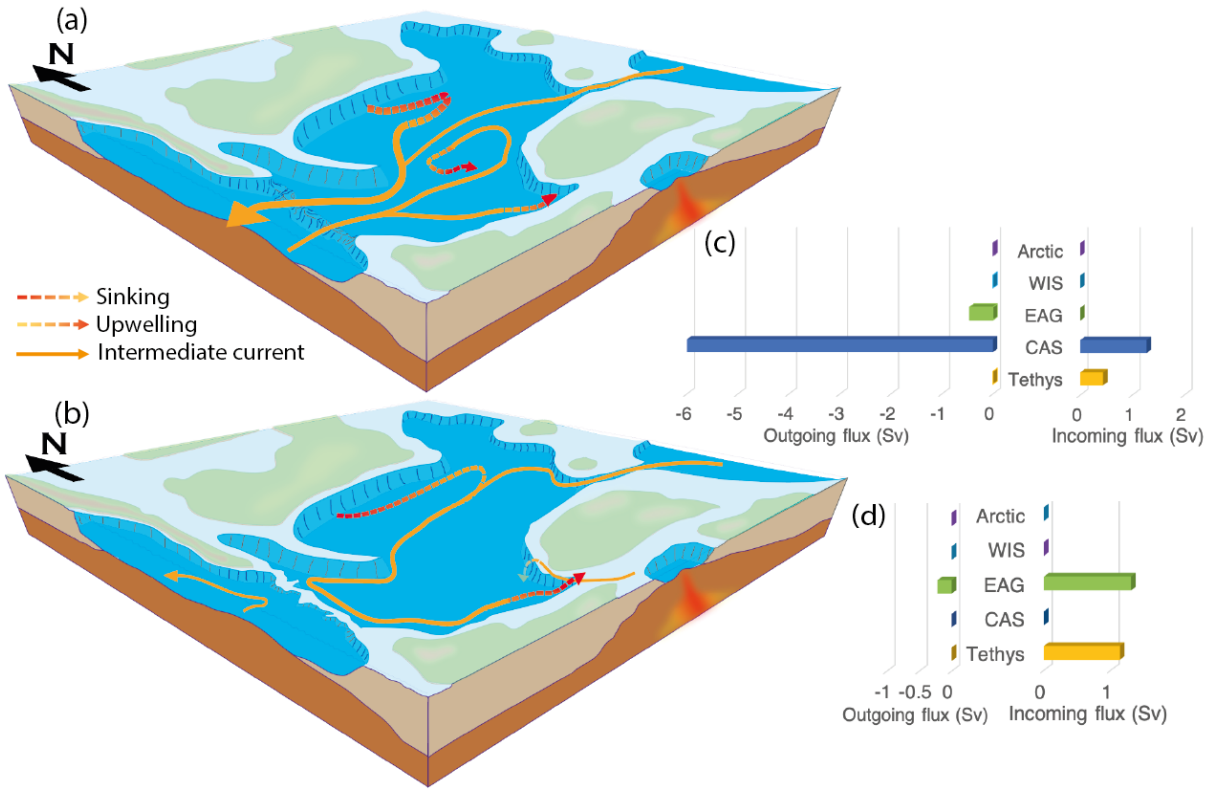

Figure 7: Schematic representation of intermediate circulation in the Central Atlantic for (a) DeepCAS and IntermediateCAS simulations and (b) ShallowCAS simulation. (c) Incoming/outgoing water fluxes (Sverdrups – Sv) for DeepCAS simulations. Fluxes for IntermediateCAS simulations are similar. (d) Incoming/outgoing water fluxes for ShallowCAS simulation.

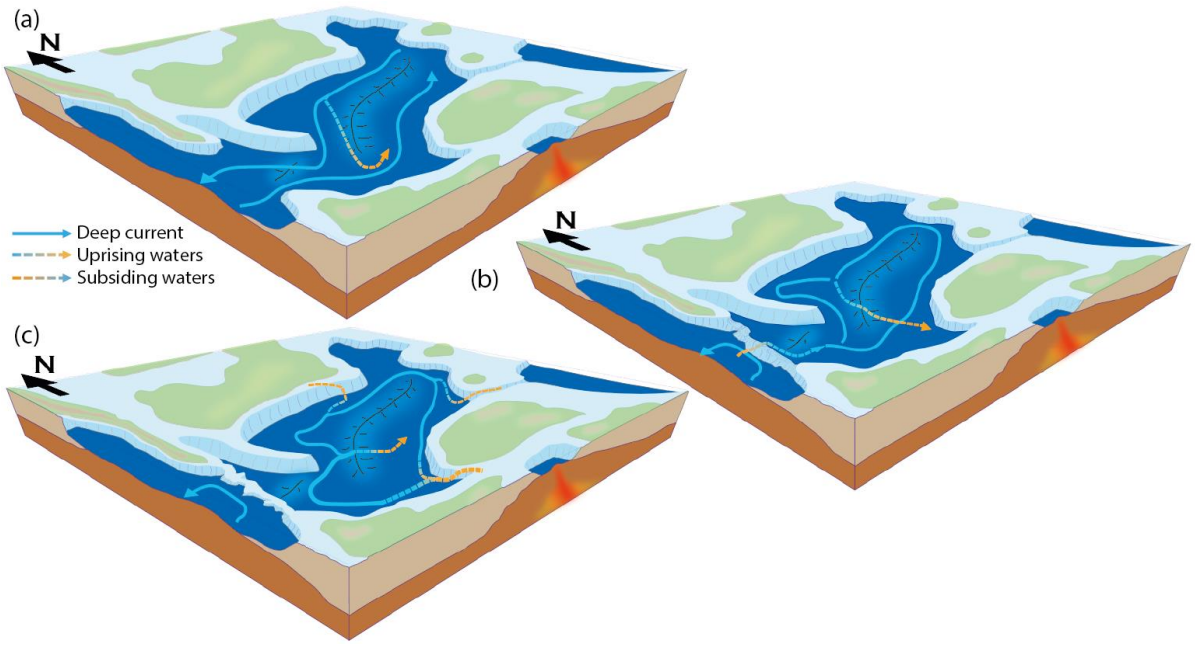

Figure 8: Schematic representation of deep circulation in the Central Atlantic for (a) DeepCAS, (b) IntermediateCAS and (c) ShallowCAS simulations.

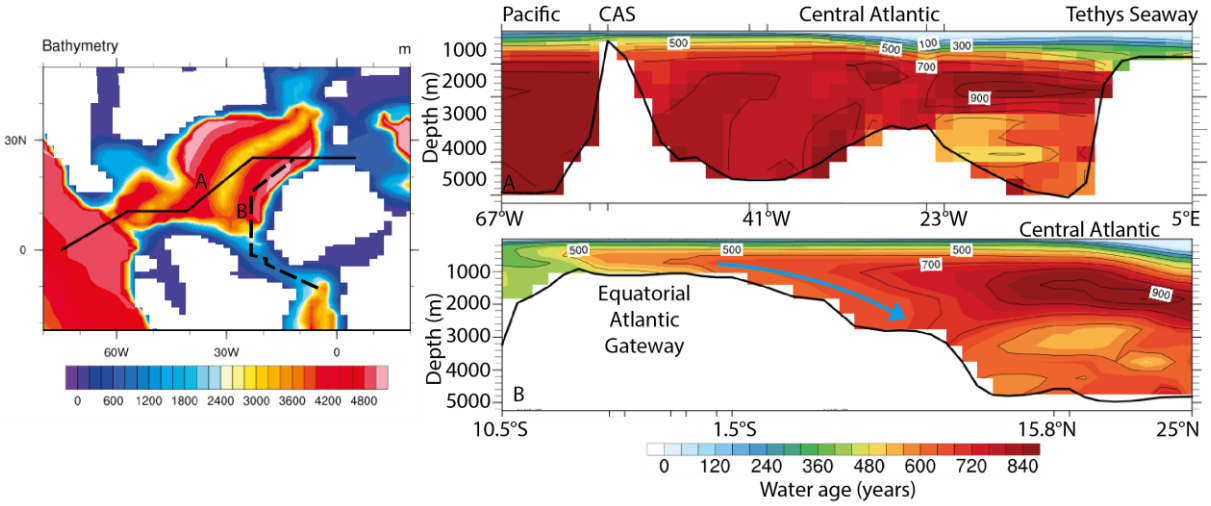

Figure 9: Vertical sections of the water age (years) for the ShallowCAS simulation. The Section A is through the Tethys seaway and the section B through the Equatorial Atlantic Gateway (EAG). Blue arrow North of the EAG (section B) indicates intermediate water subsidence from the EAG to the Central Atlantic. No subsidence is observed near the Tethys Seaway.

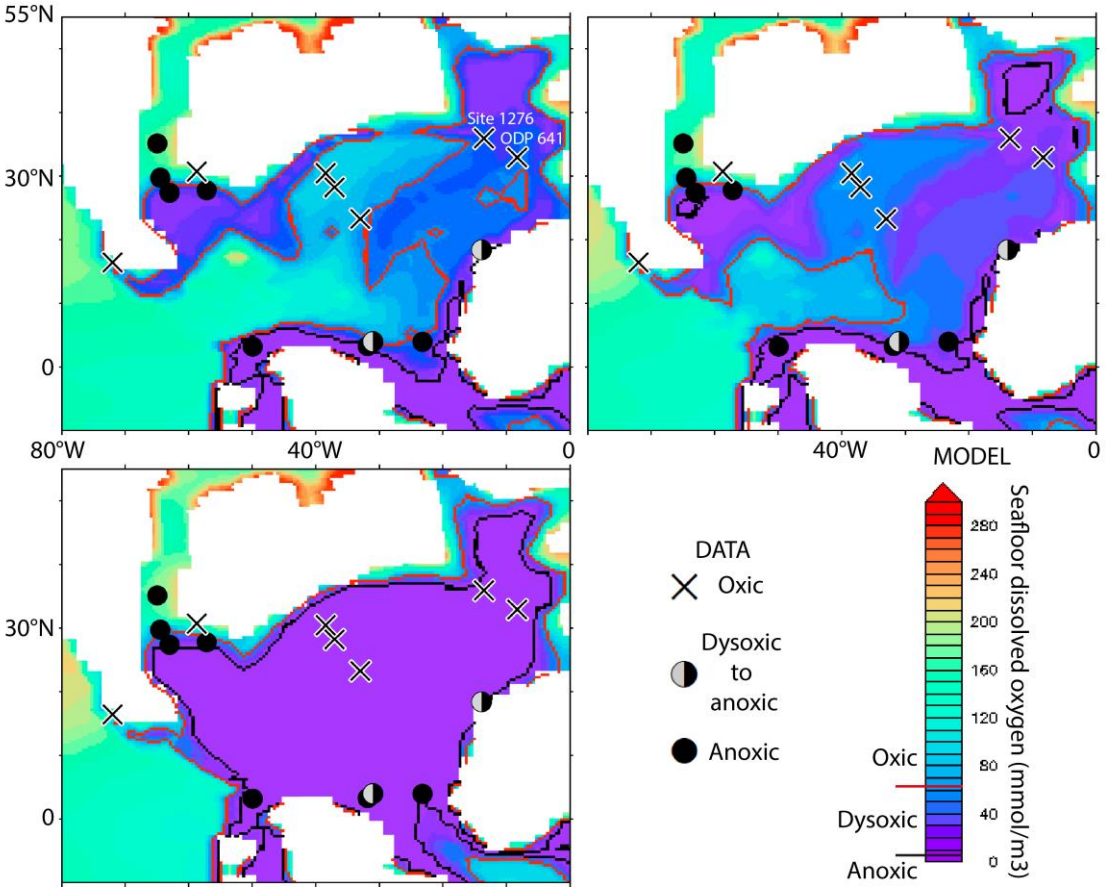

Figure 10: Seafloor dissolved oxygen concentration (mmol/m^3) for (a) DeepCAS, (b) IntermediateCAS and (c) ShallowCAS simulations. Red, and black lines correspond to hypoxia and anoxia limits, respectively. Waters are hypoxic for oxygen concentrations below 62.5 mmol.m^{-3} and anoxic below 6.5 mmol.m^{-3} (see color scale)
Crosses and dots correspond to Pre-OAE2 redox data (see discussion). Sites IODP 1276 and ODP 641 exhibit a data-model mismatch addressed in the discussion.

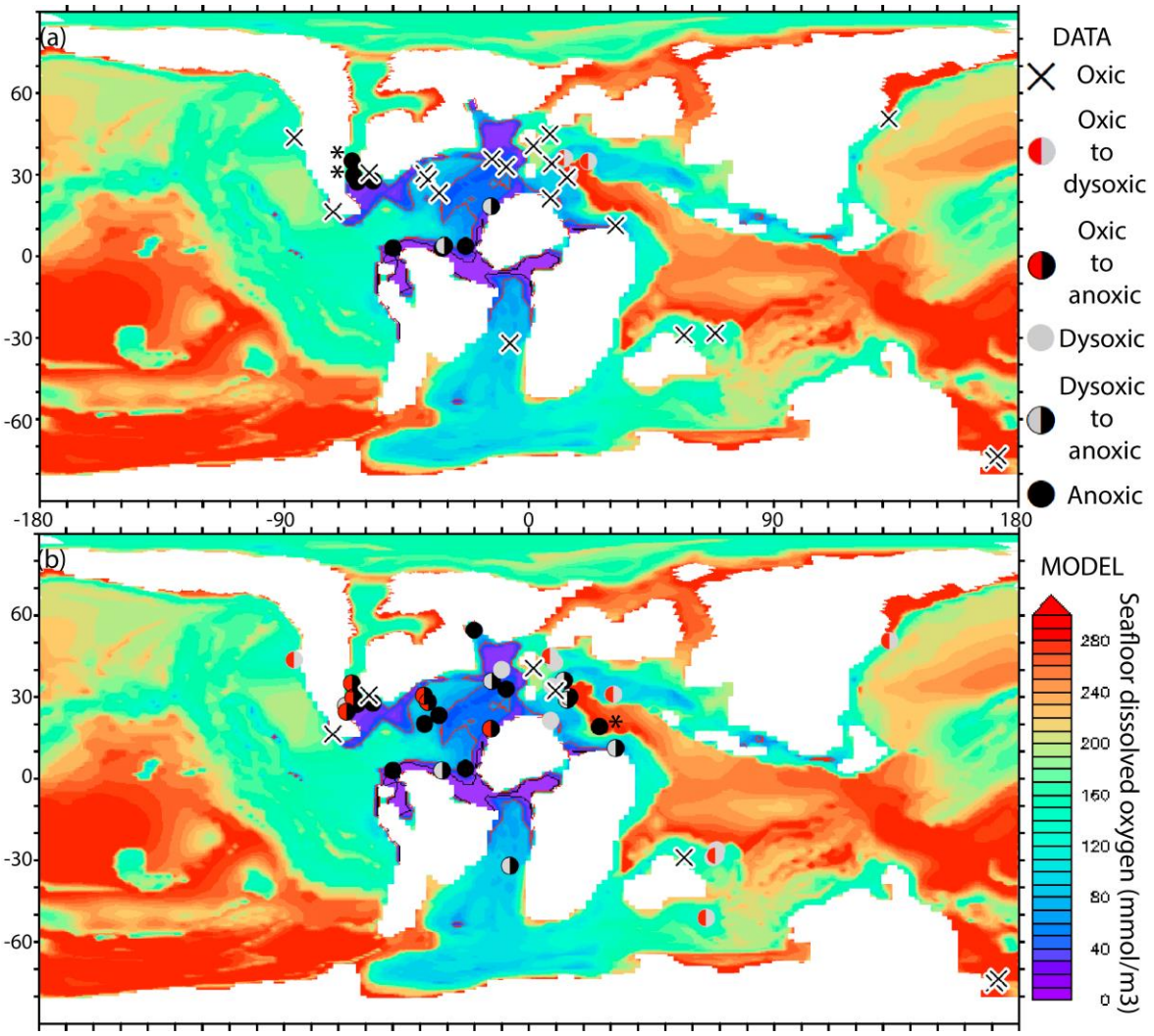

Figure 11: Seafloor dissolved oxygen concentration for the DeepCAS simulation (mmol.m^{-3}) compared with redox data for (a) the pre-OAE2 period and (b) the OAE2. The black and red lines indicate the limits of anoxia and dysoxia, respectively. Except in the central Atlantic, oxygen modelling results for IntermediateCAS and Shallow CAS are similar (See Supplementary Figure S9). Dots emphasized with asterisks correspond to model-data mismatches discussed.

Figure 1.

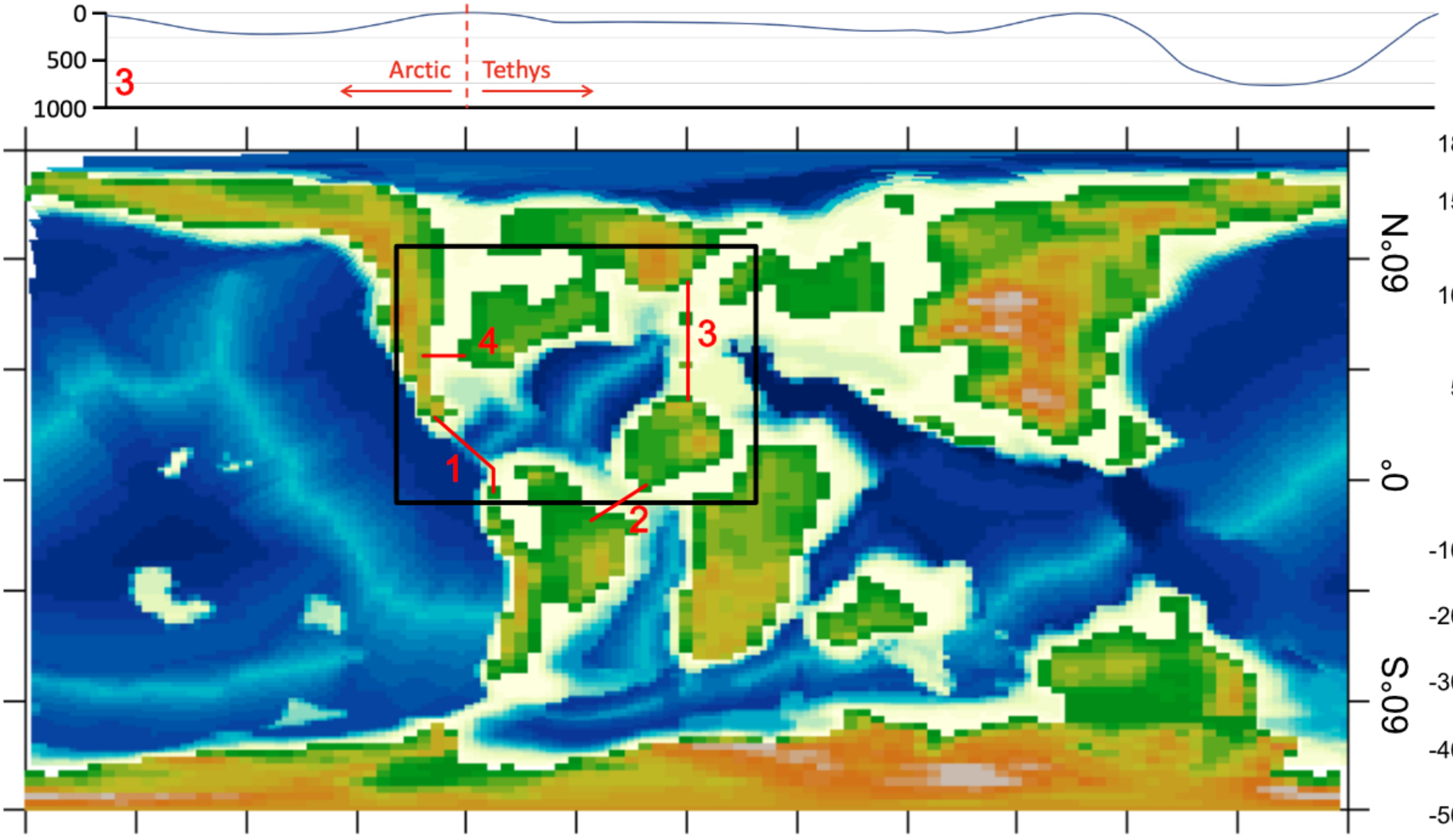
0
500
1000
3
Arctic
Tethys
90°N
0°
60°S
1
2
3
4
1800
1500
1000
500
0
-1000
-2000
-3000
-4000
-5000
Bathymetry / Topography (meters)

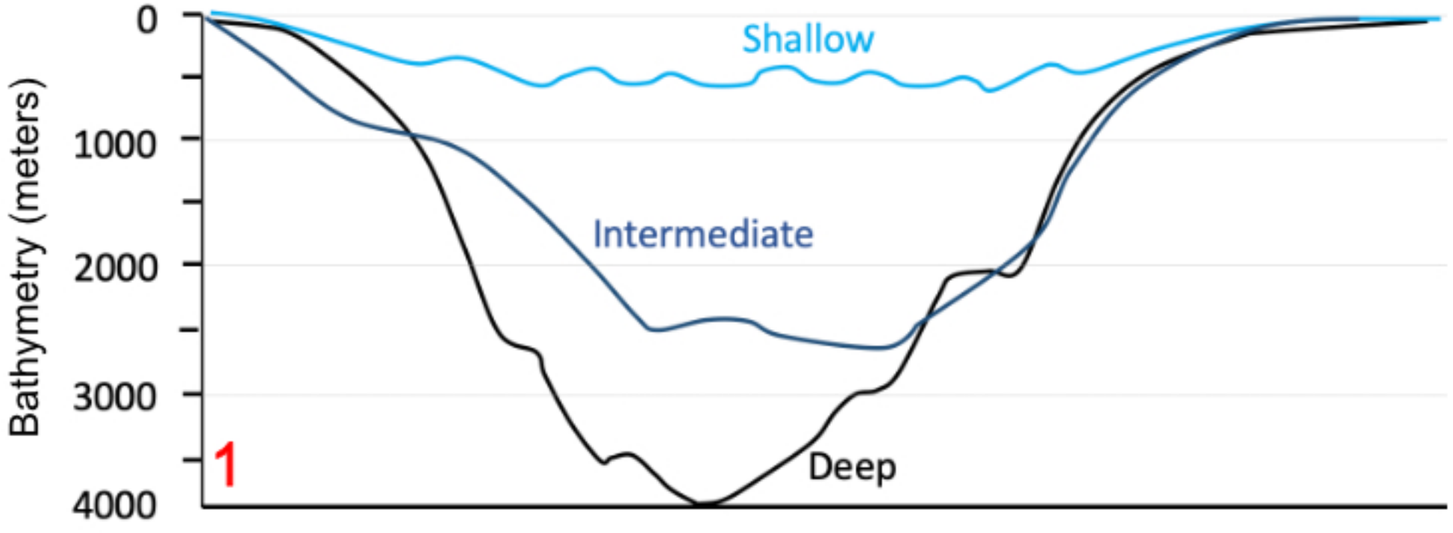
0
1000
2000
3000
4000
Bathymetry (meters)
Shallow
Intermediate
Deep
1

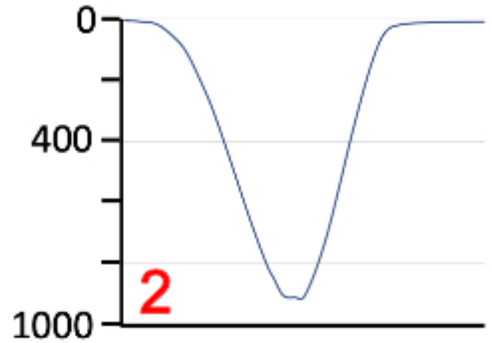
0
400
1000
2


0
200
4

Figure 2.

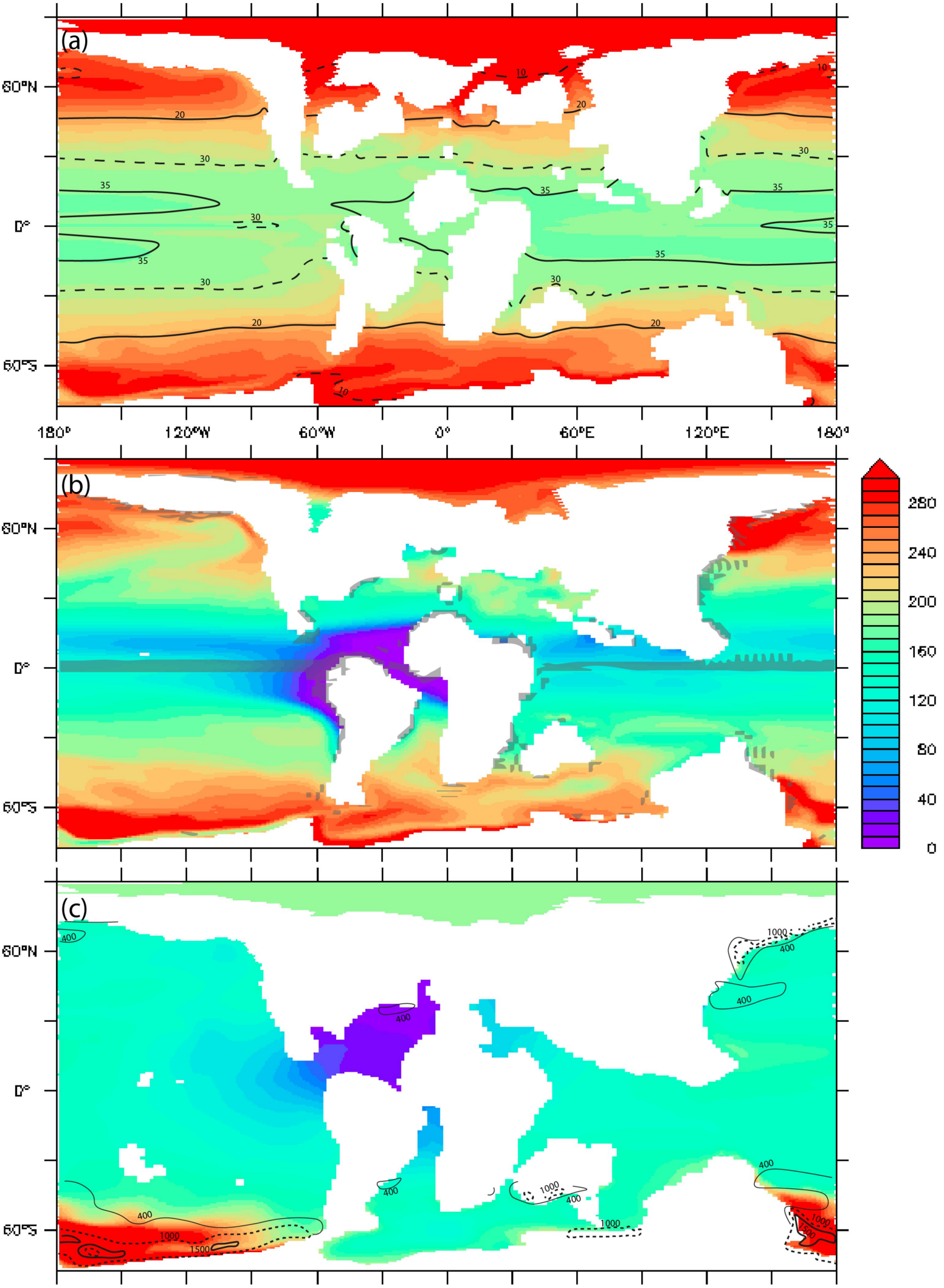
(a)
60°N
0°
60°S
180°
120°W
60°W
0°
60°E
120°E
180°
10
20
30
35
(b)
60°N
0°
60°S
280
240
200
160
120
80
40
0
(c)
60°N
0°
60°S
400
1000
1500

Figure 3.

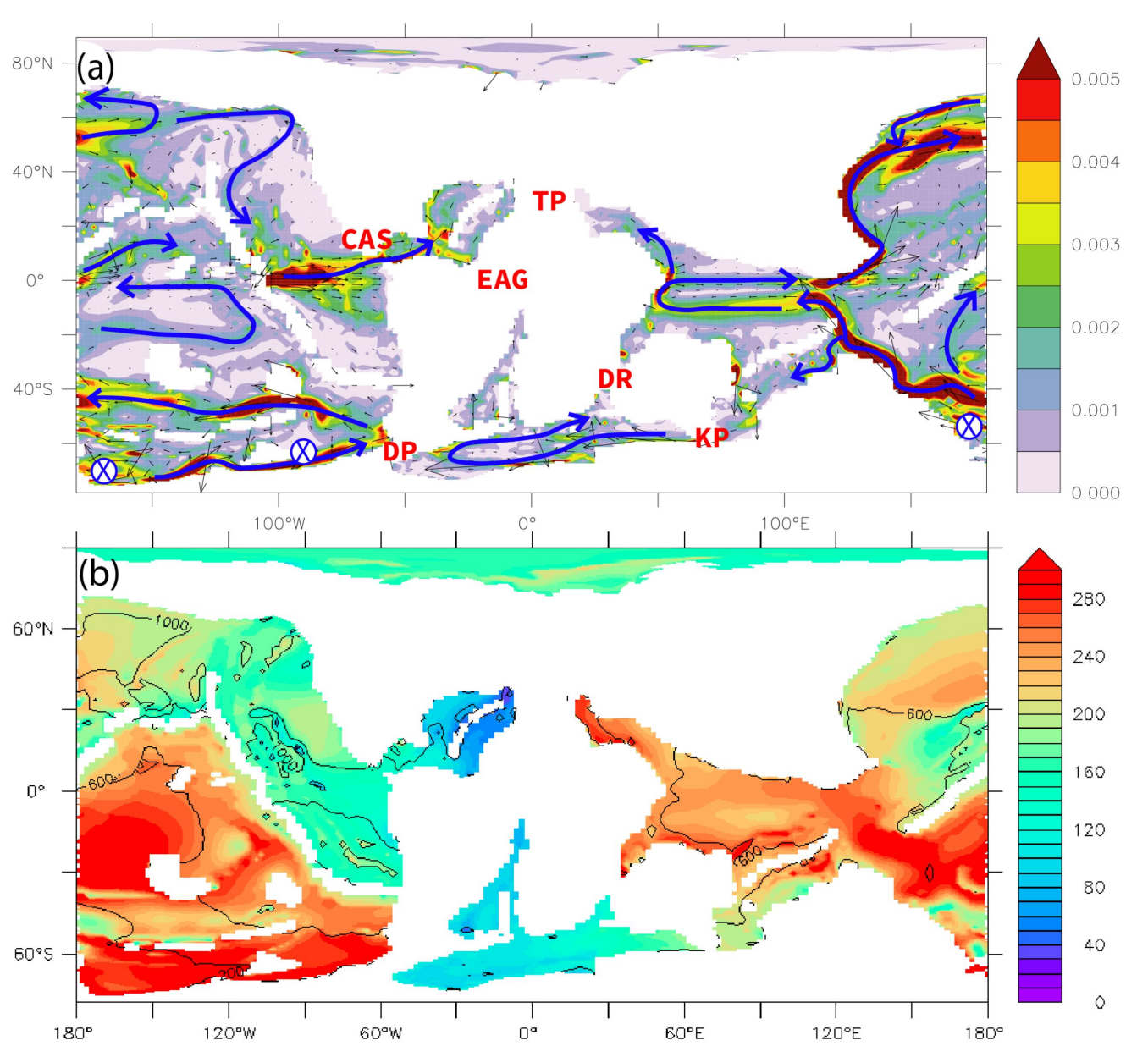
(a)
80°N
40°N
0°
40°S
100°W
0°
100°E
TP
CAS
EAG
DR
DP
KP
0.005
0.004
0.003
0.002
0.001
0.000
(b)
60°N
0°
60°S
1000
600
200
180°
120°W
60°W
0°
60°E
120°E
180°
280
240
200
160
120
80
40
0

Figure 4.

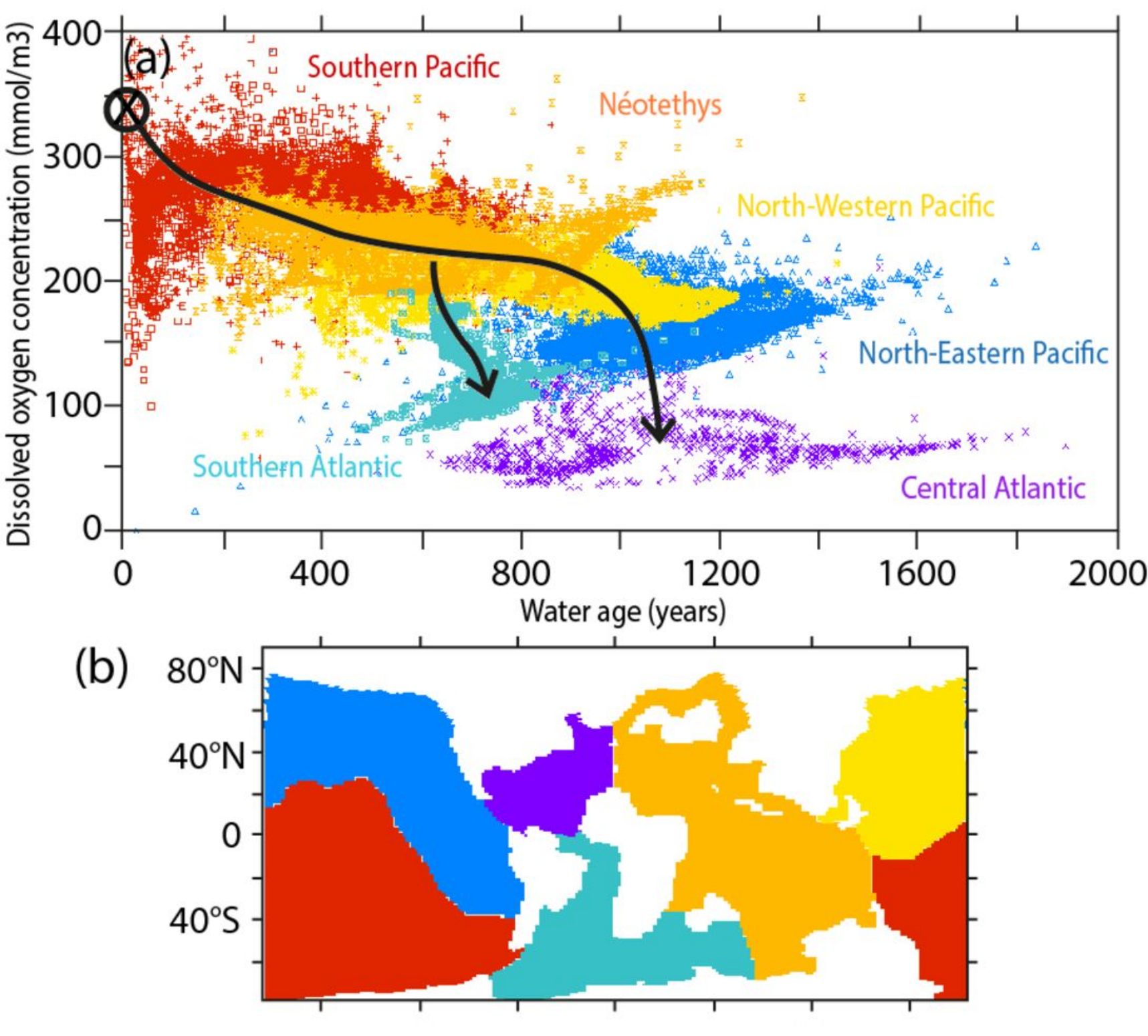
(a)
Southern Pacific
Néotethys
North-Western Pacific
North-Eastern Pacific
Southern Atlantic
Central Atlantic
Dissolved oxygen concentration (mmol/m3)
400
300
200
100
0
0
400
800
1200
1600
2000
Water age (years)
(b)
80°N
40°N
0
40°S

Figure 5.

(a)

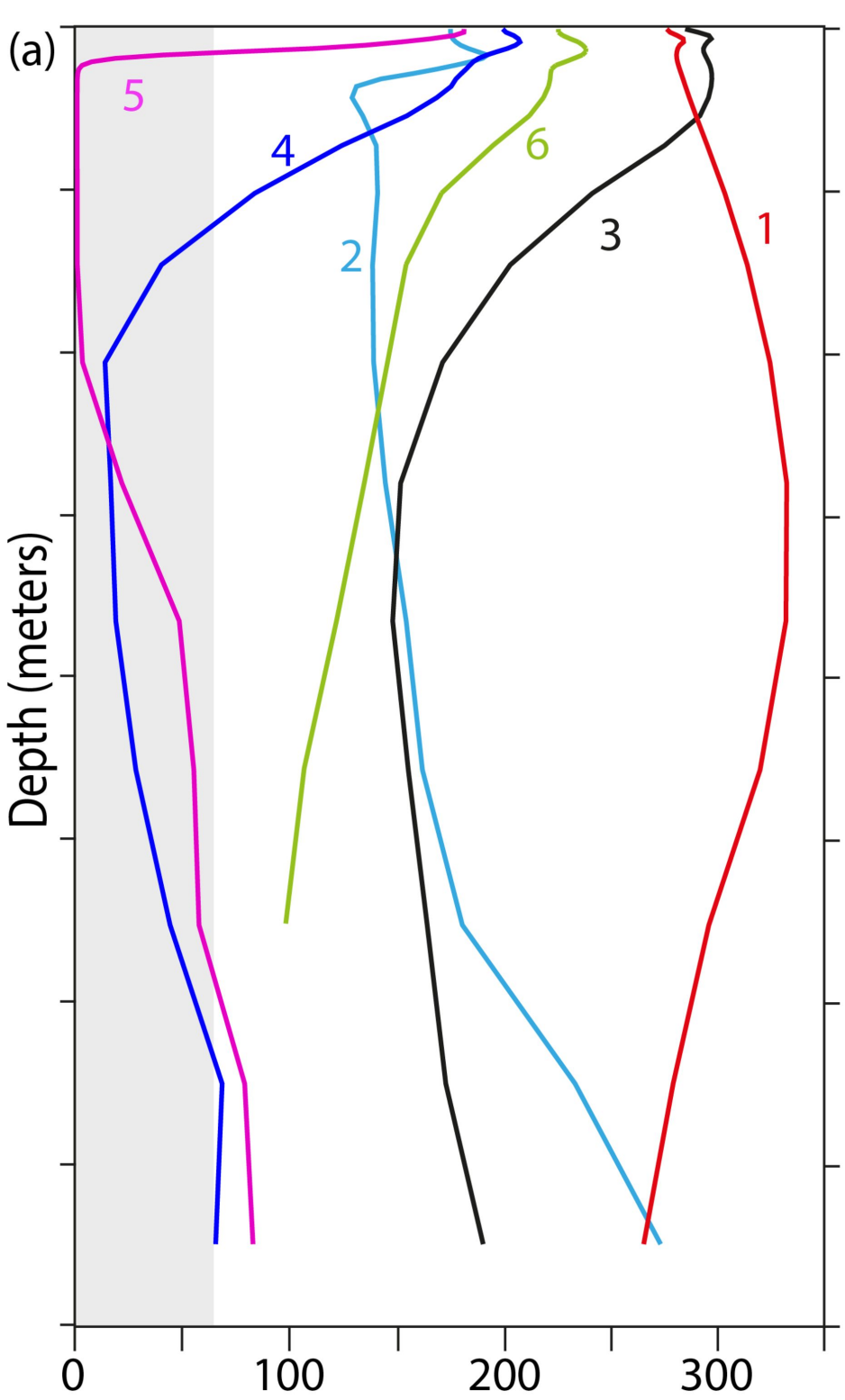
5
4
6
2
3
1
0
1000
2000
3000
4000
Depth (meters)
0
100
200
300
Dissolved oxygen concentration (mmol/m3)

(b)

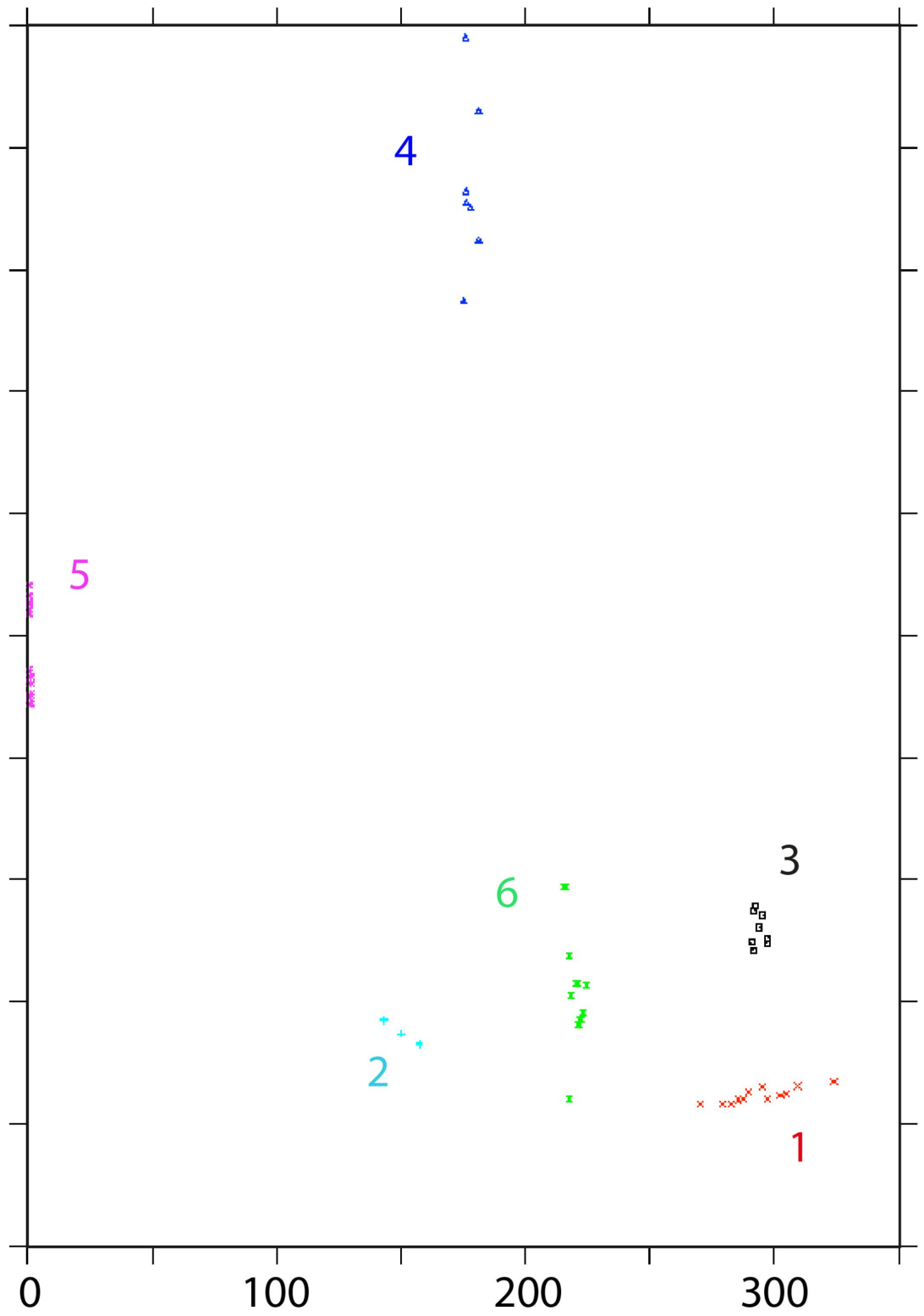
500
400
300
200
100
Marine Productivity (gC/m3/yr)
4
5
3
6
2
1
0
100
200
300
Dissolved oxygen concentration (mmol/m3)

(c)

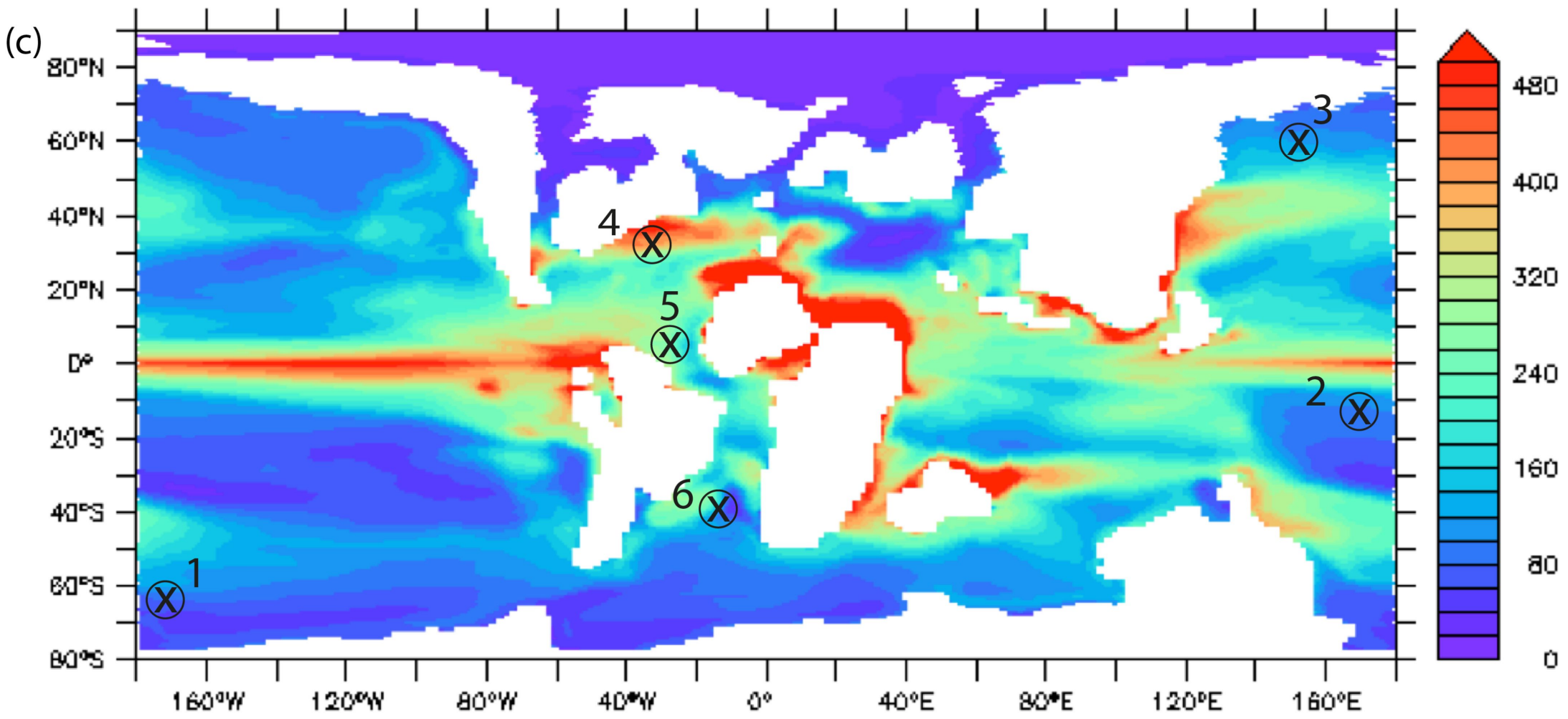
80°N
60°N
40°N
20°N
0°
20°S
40°S
60°S
80°S
160°W
120°W
80°W
40°W
0°
40°E
80°E
120°E
160°E
4
5
3
6
2
1
480
400
320
240
160
80
0
Marine Productivity (gC/m3/yr)

Figure 6.

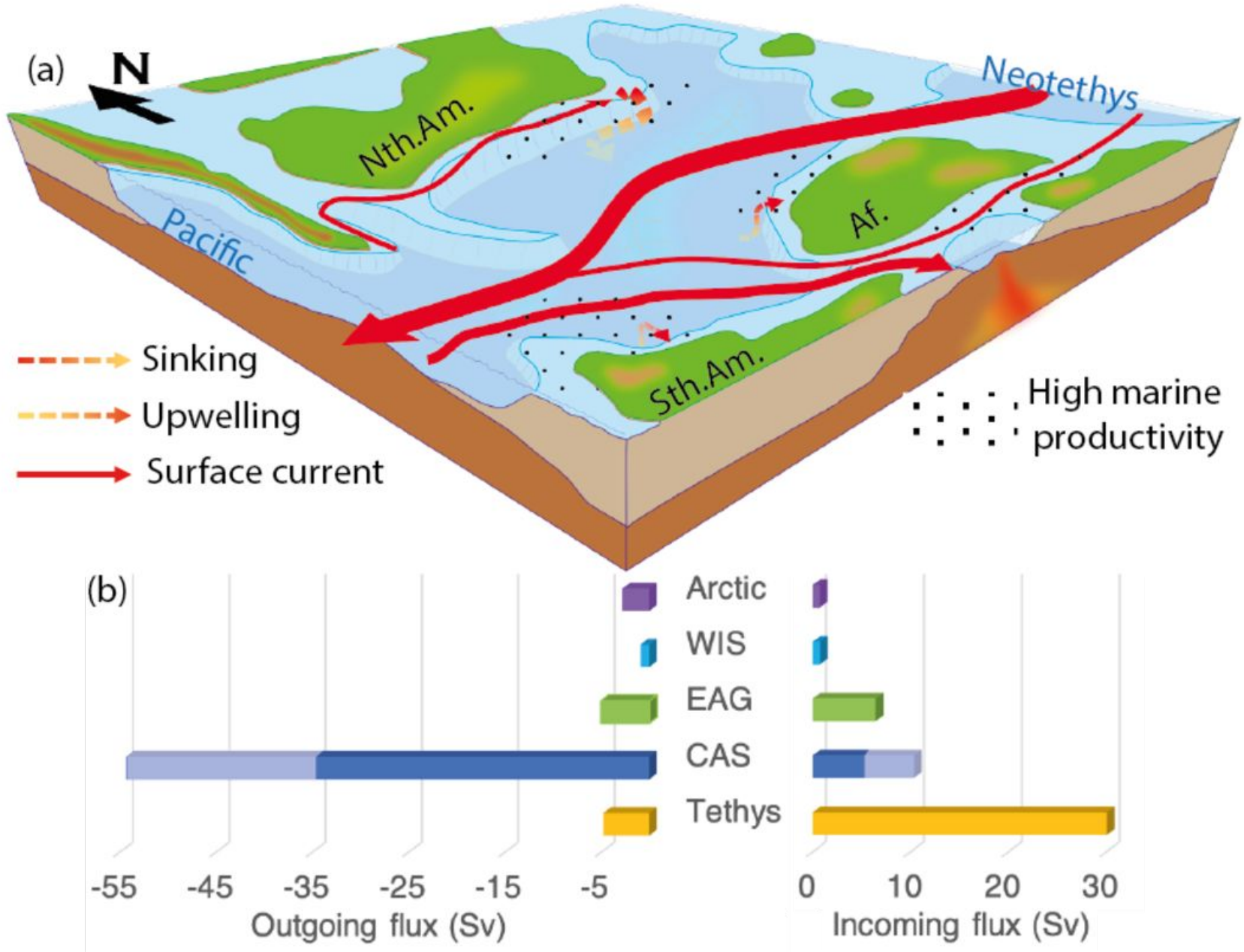
(a)
N
Nth.Am.
Neotethys
Pacific
Af.
Sth.Am.
Sinking
Upwelling
Surface current
High marine productivity
(b)
Arctic
WIS
EAG
CAS
Tethys
-55
-45
-35
-25
-15
-5
Outgoing flux (Sv)
0
10
20
30
Incoming flux (Sv)

Figure 7.

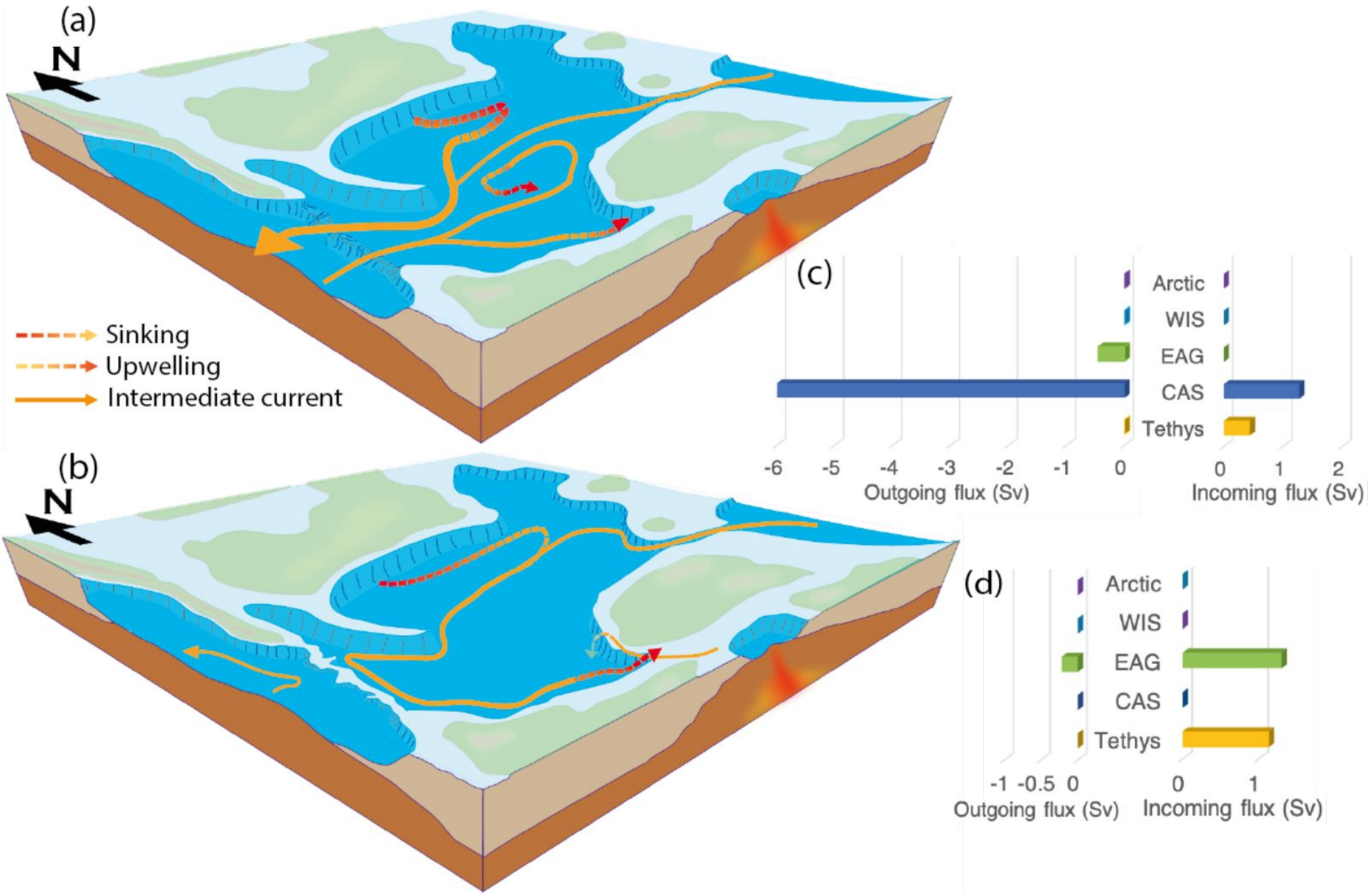
(a)
N
Sinking
Upwelling
Intermediate current
(b)
N
(c)
Arctic
WIS
EAG
CAS
Tethys
-6 -5 -4 -3 -2 -1 0
Outgoing flux (Sv)
0 1 2
Incoming flux (Sv)
(d)
Arctic
WIS
EAG
CAS
Tethys
-1 -0.5 0
Outgoing flux (Sv)
0 1
Incoming flux (Sv)

Figure 8.

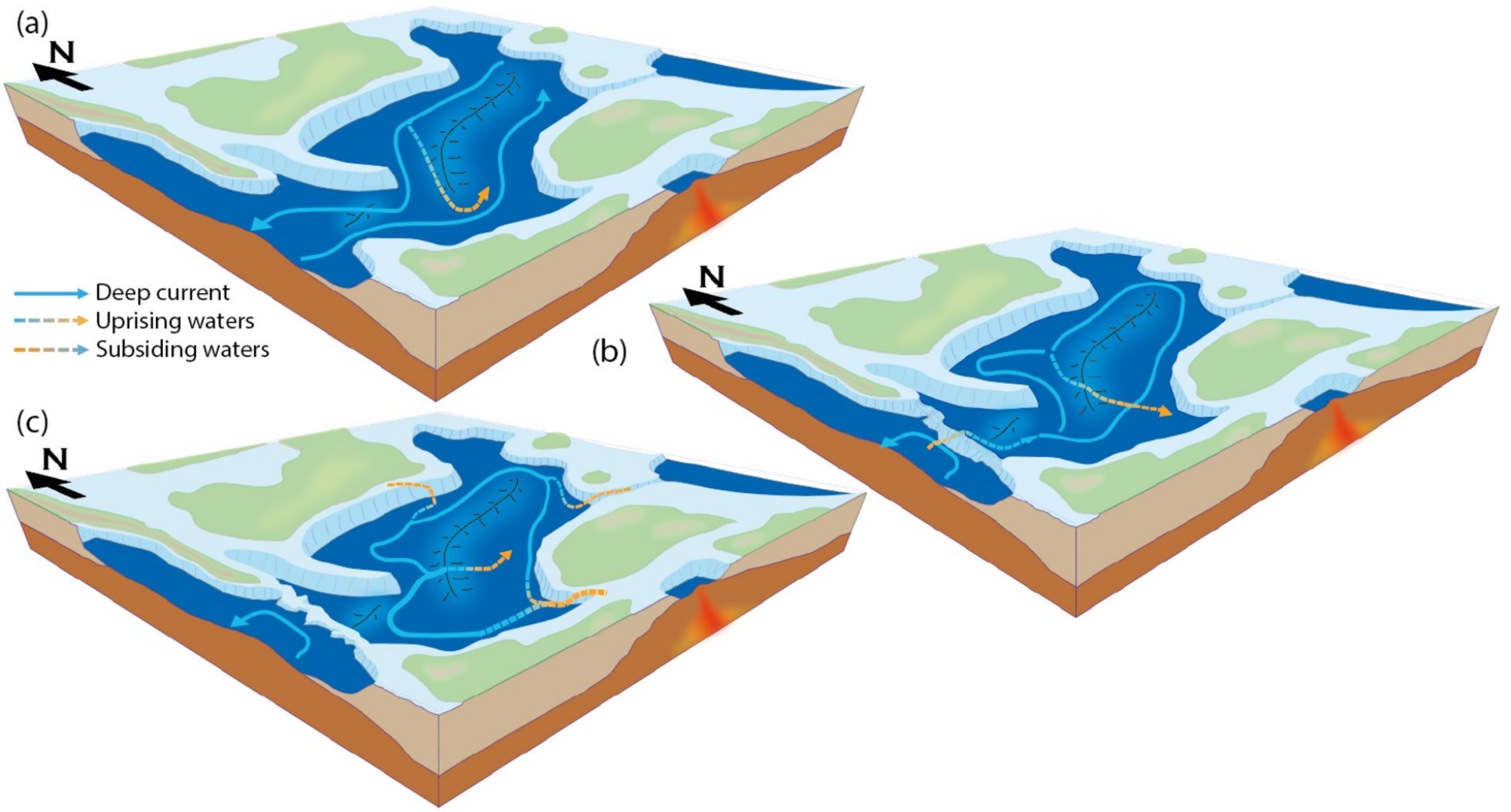
(a)
N
Deep current
Uprising waters
Subsiding waters
(b)
N
(c)
N

Figure 9.

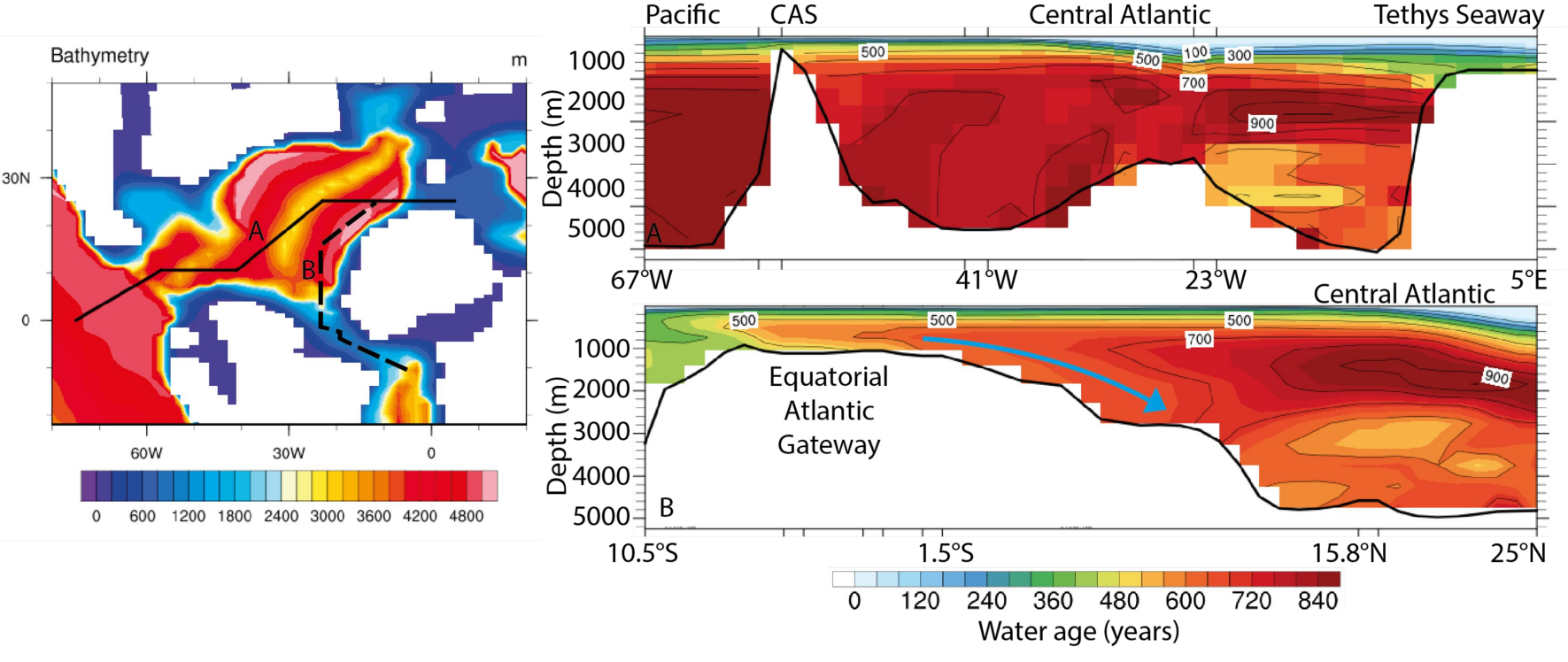
Bathymetry
m
30N
0
A
B
60W
30W
0
0 600 1200 1800 2400 3000 3600 4200 4800
Pacific
CAS
Central Atlantic
Tethys Seaway
Depth (m)
1000
2000
3000
4000
5000
500
500
100
300
700
900
A
67°W
41°W
23°W
5°E
Central Atlantic
500
500
500
700
900
Equatorial
Atlantic
Gateway
B
10.5°S
1.5°S
15.8°N
25°N
0 120 240 360 480 600 720 840
Water age (years)

Figure 10.

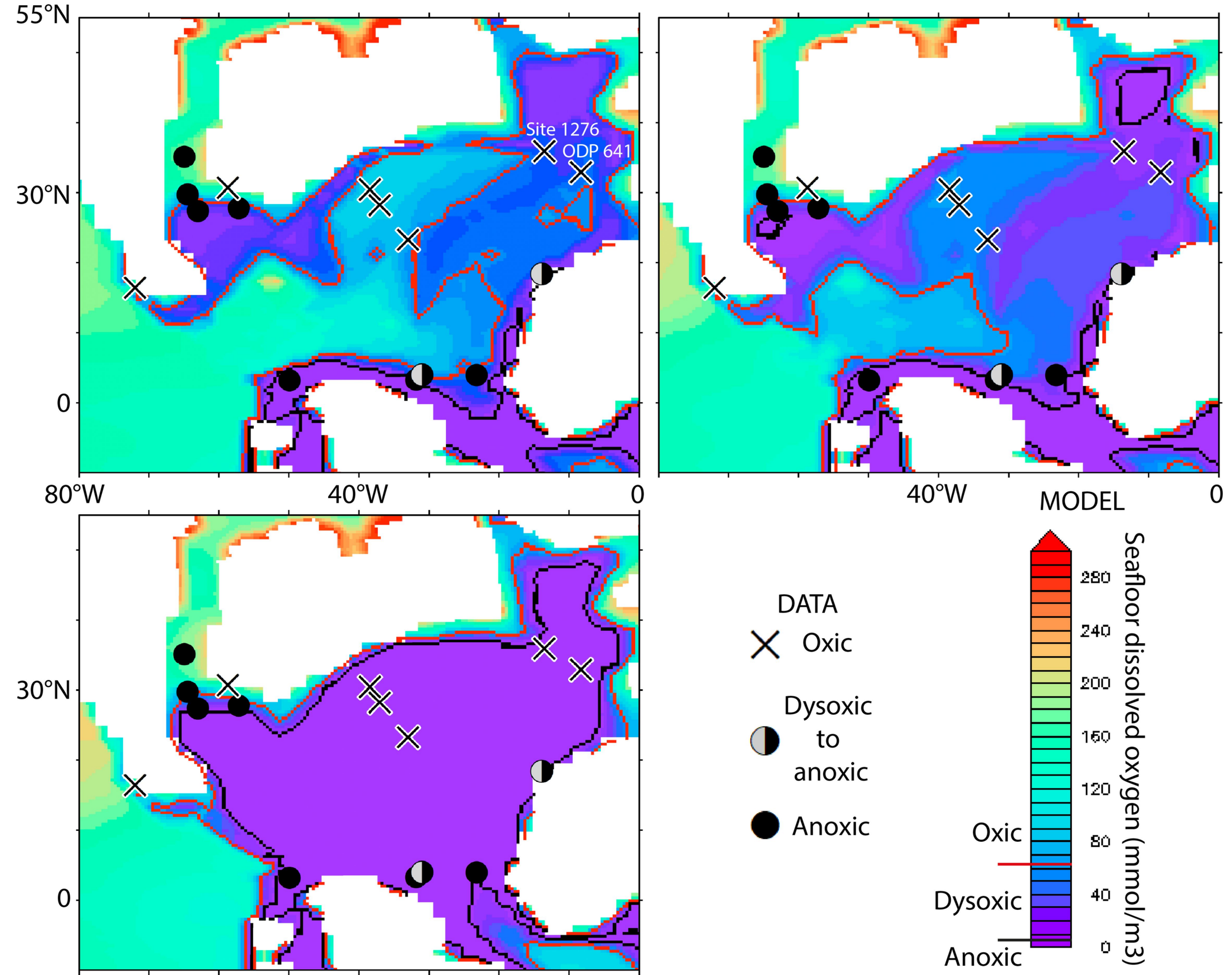
55°N
30°N
0
80°W
40°W
0
Site 1276
ODP 641
40°W
0
MODEL
30°N
0
DATA
Oxic
Dysoxic to anoxic
Anoxic
Seafloor dissolved oxygen (mmol/m3)
280
240
200
160
120
80
40
0
Oxic
Dysoxic
Anoxic

Figure 11.

(a)

60
30
0
-30
-60

DATA

Oxic

Oxic to dysoxic

Oxic to anoxic

Dysoxic

Dysoxic to anoxic

Anoxic

-180
-90
0
90
180

(b)

60
30
0
-30
-60

MODEL

Seafloor dissolved oxygen (mmol/m3)

280
240
200
160
120
80
40
0